AD-A242 749

DTIC

Report on the
Second Gulf of Cadiz Expedition Workshop
April 9–11, 1991
Applied Physics Laboratory
University of Washington

by

M. D. Allison, I. Ambar, G. C. Johnson, M. A. Kennelly, H. König, E. L. Kunze,
R. Lueck, M. O. Baringer, M. D. Prater, J. F. Price, T. B. Sanford,
K. L. Schultz Tokos, J. Verrall, J. C. Wesson, and W. Zenk

91-15817

Report on the
Second Gulf of Cadiz Expedition Workshop

April 9–11, 1991
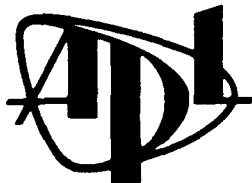Applied Physics Laboratory
University of Washington

by

M. D. Allison, I. Ambar, G. C. Johnson, M. A. Kennelly, H. König, E. L. Kunze,
R. Lueck, M. O. Baringer, M. D. Prater, J. F. Price, T. B. Sanford,
K. L. Schultz Tokos, J. Verrall, J. C. Wesson, and W. Zenk

Applied Physics Laboratory   University of Washington
1013 NE 40th Street   Seattle, Washington 98105–6698

Statement A per telecon
Robert Silverman ONR
1107 NE 45th St. Suite 410
Seattle, WA 98105-4631
NWW 11/21/91

Acknowledgments

TABLE OF CONTENTS

LIST OF FIGURES

LIST OF TABLES

1. INTRODUCTION

A workshop on the scientific results of the ONR-sponsored Gulf of Cadiz Expedition was held April 9–11, 1991, at the Applied Physics Laboratory, University of Washington. The objectives of the Gulf of Cadiz Expedition were to observe the vortices shed in the wake of Ampere Seamount, to survey Meddies formed by the Mediterranean outflow near Cape St. Vincent, Portugal, and to study the structure and dynamics of the outflow plume west of the Strait of Gibraltar. The operational areas for the expedition are shown in Figure 1.1. During the Expedition (September 4–28, 1988), velocity, hydrographic, and dissipation measurements were made using a variety of instrument systems (XCP, XDP, XBT, XSV, CTD, and ADCP). Table 1.1 lists the data types, number of casts, drops, or observations made, the percentage of good drops (expendables only), and the reports or publications describing the processing of each particular data type.

Investigators from APL-UW, WHOI, JHU/CBI, the University of Lisbon, and the Spanish Institute of Oceanography participated in the expedition. A workshop to discuss preliminary results of the expedition was held at the Woods Hole Oceanographic Institution in October 1989. The agenda for the present workshop is given in Appendix A. Table 1.2 lists present publications according to research objective, and Appendix B contains a complete list of contributions resulting from the expedition. Participants in the April 1991 workshop are given in Appendix C. Appendix D lists past and future workshops.

The following sections will present highlights of the presentations given at the workshop. Results and plans for related work are also included.

2. AMPERE SEAMOUNT COMPONENT

2.1 Measurements of Ertel Vorticity Finestructure near Ampere Seamount

Recently, it has been suggested that the oceanic fine scale is dominated by stratified 2-D turbulence (vortical mode) rather than by internal gravity waves as traditionally thought; while large-scale flows can be distinguished on the basis of frequency, high-wavenumber structure is readily Doppler-shifted so its dynamics cannot be readily discerned from simple time series. The Ertel vorticity can be used to distinguish between these two balances since anomalies of this quantity can be associated with stratified 2-D turbulence but not with internal waves. The Ertel vorticity can be approximated as

$$\prod = (f + \nabla \times V) \cdot \nabla (B + b) = f\bar{N}^2 + fb_z + \zeta\bar{N}^2 + \zeta b_z + b_x v_z - b_y u_z$$

and is comprised of a background $f\bar{N}^2$, two linear anomaly terms (stretching fb_z and relative vorticity $\zeta\bar{N}^2$), and three nonlinear anomalies. For linear internal waves, the stretching and relative vorticity terms cancel. Another useful distinguishing characteristic is that the vortical mode has higher relative vorticity than horizontal convergence; near-

Table 1.1. Gulf of Cadiz Data.

Overview			Kennelly, Dunlap, Sanford, Kunze, Prater, and Drever, 1989: The Gulf of Cadiz Expedition: R/V *Oceanus* Cruise 202. APL-UW TR 8914. Ambar, Bower, Cantos-Figuerola, Kennelly, Kunze, Lueck, Baringer, Parrilla, Prater, Price, Richardson, Sanford, and Tokos, 1990: Report on the Gulf of Cadiz Expedition Workshop, Oct. 1 & 2, 1989. APL-UW TM 9-90.
Drifter	7 tracks		Kennelly, Dunlap, Sanford, Kunze, Prater, and Drever, 1989: The Gulf of Cadiz Expedition: R/V *Oceanus* Cruise 202. APL-UW TR 8914. Drever and Kennelly, 1991: Simple Low-Cost Drogued Drifter To be submitted to *J. Atmos. Oceanic Technol.*
XCP	184	87%	Kennelly, Prater, Dunlap, Kunze, and Sanford, 1989: XCP Data from the Gulf of Cadiz Expedition: R/V APL-UW TR 8925. Prater, 1991: A Method for Depth and Temperature Correction of Expendable Probes, *J. Atmos. Oceanic Technol.* (accepted).
XBT T-5 T-6 T-7	182 7 40	82% 100% 90%	Kennelly, Prater, and Sanford, 1989: XBT and XSV Data from the Gulf of Cadiz Expedition: R/V *Oceanus* Cruise 202. APL-UW TR 8920.
XSV XSV-02 XSV-03	52 3	79% 100%	Kennelly, Prater, and Sanford, 1989: XBT and XSV Data from the Gulf of Cadiz Expedition: R/V *Oceanus* Cruise 202. APL-UW TR 8920.
XDP	61		Lynch and Lueck, 1989: Expendable Dissipation Profiler (XDP) Data from the Mediterranean Out-Flow Experiment: R/V *Oceanus* Cruise 202 Leg V. JHU-CBI TR 89-01.
CTD	148		Kennelly, Sanford, and Lehman, 1989: CTD Data from the Gulf of Cadiz Expedition: R/V *Oceanus* Cruise 202. APL-UW TR 8917.
ADCP	continuous		
Bathymetry	continuous		Digitized and merged with navigation database.
SAIL	continuous		SST, SSC, wind speed, and direction.

Table 1.2. Gulf of Cadiz Program Publications and Presentations.

OVERVIEW

Kennelly, M.A., J.H. Dunlap, T.B. Sanford, E.L., Kunze, M.D. Prater, and R.G. Drever, 1989: The Gulf of Cadiz Expedition: R/V *Oceanus* Cruise 202. APL-UW TR 8914, Applied Physics Laboratory, University of Washington, Seattle, WA, 115 pp.

Ambar, I., A. Bower, A. Cantos-Figuerola, M.A. Kennelly, E.L. Kunze, R. Lueck, M.T. O'Neil Baringer, G. Parrilla, M.D. Prater, J.F. Price, P.L. Richardson, T.B. Sanford, and K.S. Tokos, 1990: Report on the Gulf of Cadiz Expedition Workshop, Oct. 1 & 2, 1989. APL-UW TM 9-90, Applied Physics Laboratory, University of Washington, Seattle, WA, 58 pp.

AMPERE SEAMOUNT COMPONENT

Kunze, E., and T.B. Sanford, 1990: Vorticity and horizontal divergence finestructure near a seamount (abstract). *EOS Trans. AGU,* **72**(43),1419.

Kunze, E., and T.B. Sanford, 1991: Measurements of ertel vorticity finestructure in the eastern North Atlantic. To appear in *Dynamics of Oceanic Internal Gravity Waves, Proceedings, 'Aha Huliko'a Hawaiian Winter Workshop,* Peter Müller, Ed., Hawaii Institute of Geophysics.

Kunze, E., M.A. Kennelly, and T.B. Sanford, 1991: The depth dependence of shear finestructure off Point Arena and over Pioneer Seamount. To appear in *J. Phys. Oceanogr.,* **21**.

MEDDY COMPONENT

Prater, M.D., and T.B. Sanford, 1989: Observations of an intense, young Meddy (abstract), *EOS Trans. AGU,* **70**(43), 1159.

Prater, M.D., and T.B. Sanford, 1990: Generation of Meddies off Cape St. Vincent, Portugal (abstract), *Eos Trans. AGU,* **71**, 1416.

MEDITERRANEAN OUTFLOW COMPONENT

Price, J.F., and M.T. O'Neil [Baringer], 1988: The descending Mediterranean plume (abstract), *EOS Trans. AGU,* **69**(44), 1265.

Ambar, I., and J. Verrall, 1990: Dynamics of the Mediterranean water plume between the Strait of Gibraltar and Cape St. Vincent, *Proceedings of the 7th National Conference on Physics* (Portugal), p. 457. **72**(43), 1419.

Baringer, M.O., and J.F. Price, 1990: A simple model of the descending Mediterranean outflow plume. *The Physical Oceanography of Sea Straits,* L.J. Pratt, Ed., Kluwer Academic Publishers, Netherlands, 537-544.

Price, J.F., and M.O. Baringer, 1990: A model of the Denmark Strait overflow (abstract). *Annales Geophysicae,* XV General Assembly, European Geophysical Society, Copenhagen, April 23–27, 1990, p. 224.

Baringer, M.O., J.F. Price, and T.B. Sanford, 1990: Mixing in the Mediterranean outflow plume during the Gulf of Cadiz Experiment (abstract). *Annales Geophysicae,* XV General Assembly, European Geophysical Society, Copenhagen, April 23–27, 1990, p. 224.

Parrilla, G., and A. Cantos-Figuerola, 1990: The Mediterranean outflow plume during the Gulf of Cadiz Experiment (Sept 1988) (abstract). *Annales Geophysicae,* XV General Assembly, European Geophysical Society, Copenhagen, April 23–27, 1990, p. 224.
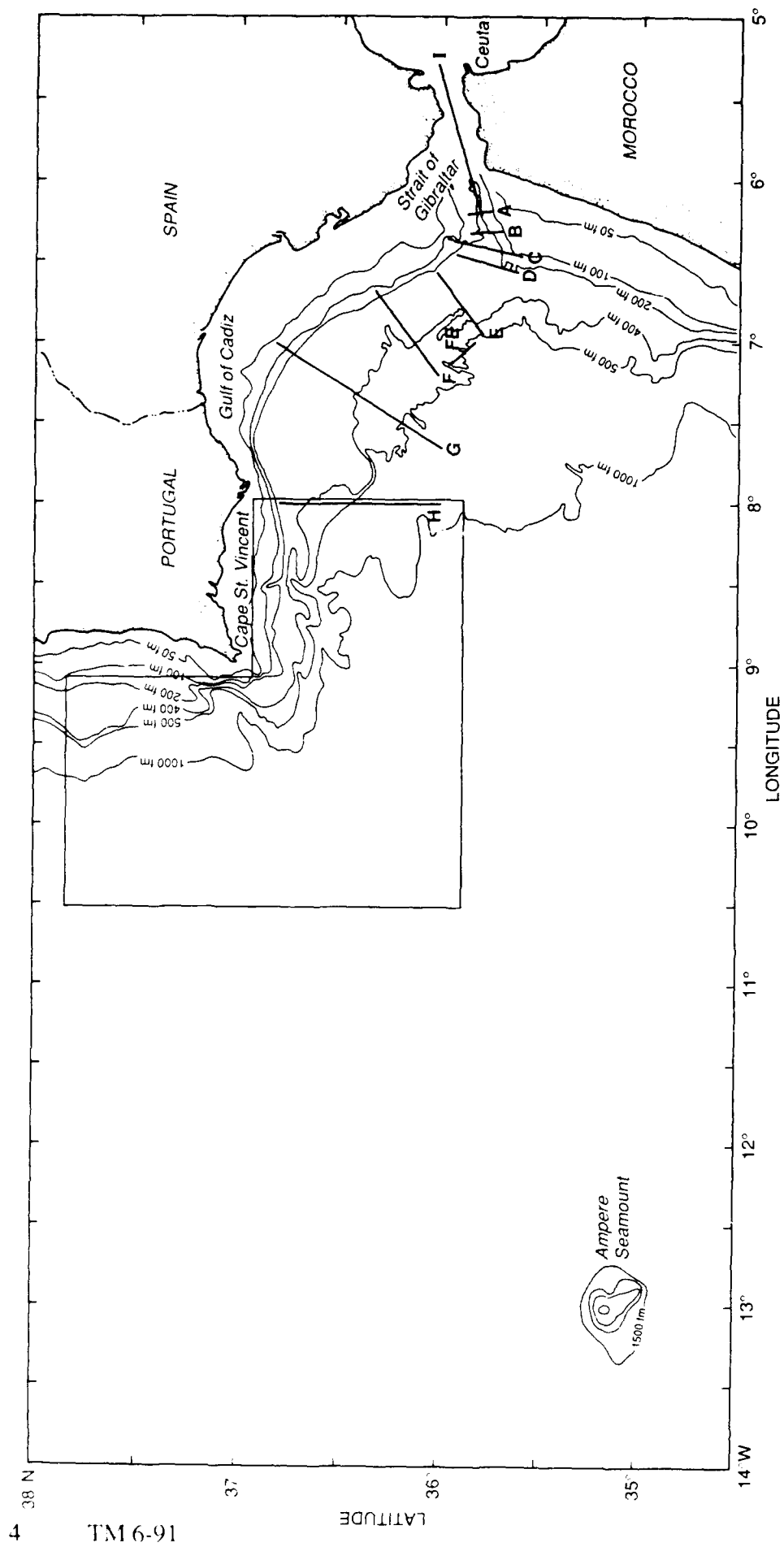
Figure 1.1. The operational areas for the Gulf of Cadiz Expedition included Ampere Seamount, the Cape St. Vincent region (boxed), and the continental slope west of the Strait of Gibraltar (sections A–I).

inertial waves have comparable vorticity and convergence, and high-frequency internal waves have much weaker vorticity than convergence.

To determine the segregation between these two dynamical regimes in the ocean, two velocity and temperature profile (XCP) surveys were conducted just east of Ampere Seamount in the eastern North Atlantic. The surveys spanned horizontal scales of 4–7 km and vertical wavelengths of 40–400 m (Burger numbers of 0.05–30). Just as on basin scales, the existing fine-scale Ertel vorticity signal is dominated by stretching (Figure 2.1.1). The dynamic signal, as characterized by the relative vorticity and horizontal convergence, is consistent with the GM internal wave model and is dominated by near-inertial waves on the resolved scales (Figure 2.1.2). The prominence of stretching indicates that Ertel vorticity finestructure is associated with nearly passive density finestructure of very low aspect ratio. This further suggests that it was not formed recently by flow separation at the seamount but might be an artifact of subduction of surface mixed layers. Anomalies of subducted water would be long lived because of the weak turbulent mixing in the main pycnocline.

Section 2.1 was contributed by Eric L. Kunze, University of Washington.
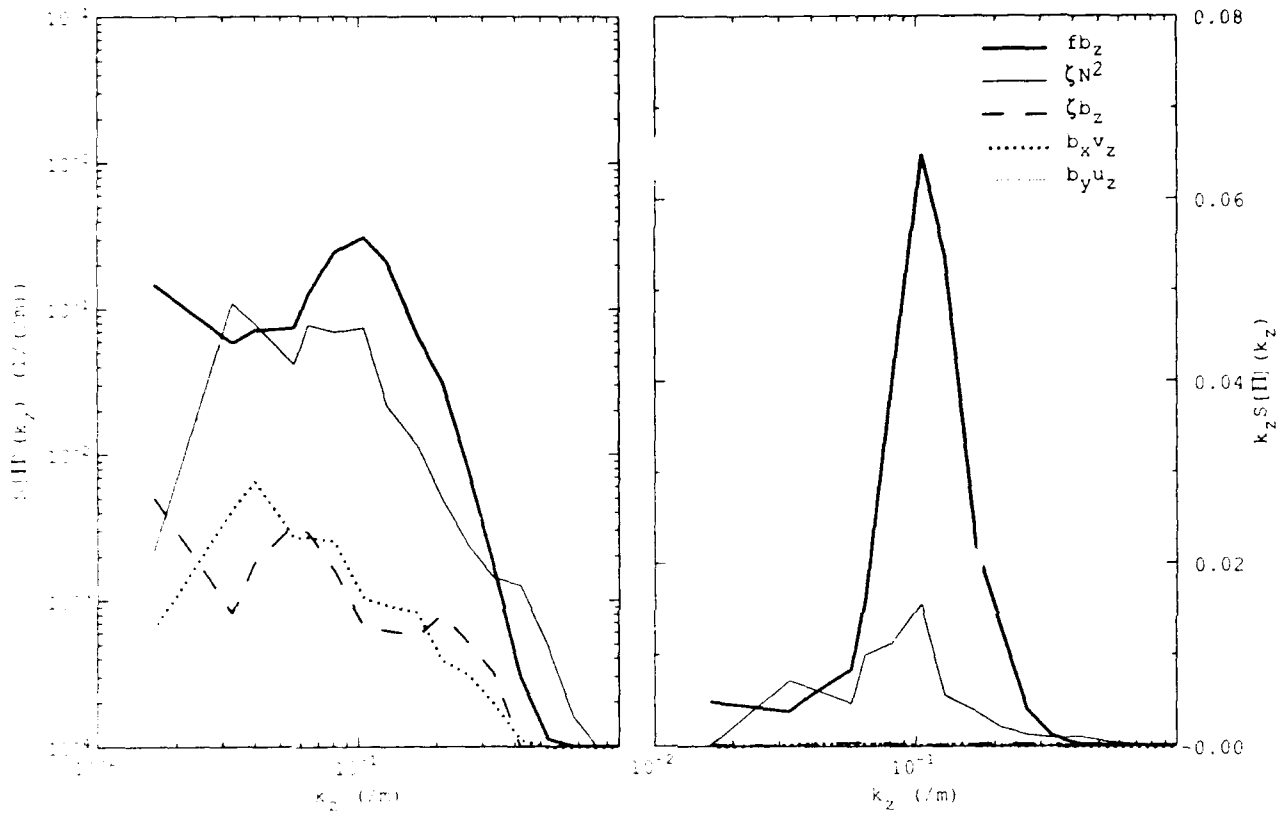
Figure 2.1.1. Vertical wavenumber spectra from survey 1 with horizontal fitting scale $\Delta r = 4$ km for the two linear and three nonlinear terms of the Ertel vorticity anomaly: stretching fb_z, relative vorticity $(v_x - u_y)\overline{N}^2$, $(v_x - u_y)b_z$, twisting $b_x v_z$, and twisting $-b_y u_z$. The spectra are presented in both log-log (left) and variance-preserving (right) forms. The stretching peak at 60-m wavelength contains an order of magnitude more variance than the other terms and thus cannot be explained by internal waves. At lower wavenumbers ($\lambda_z > 100$ m), vorticity and stretching become comparable.
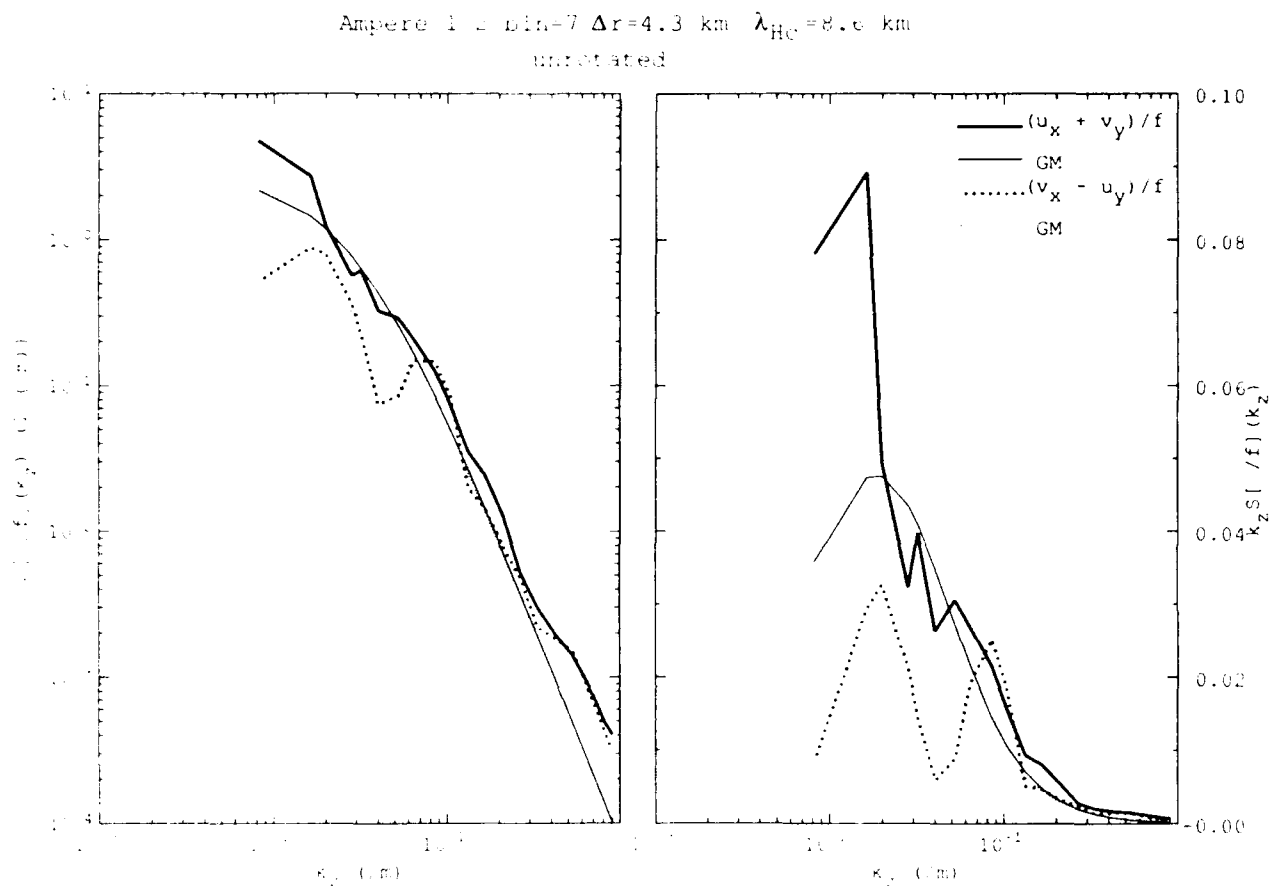
Figure 2.1.2. Comparison of the observed vertical wavenumber spectra for horizontal convergence and relative vorticity from survey 1 (thick curves) with the GM model integrated to horizontal wavenumbers of $\pi/8.6$ km^{-1} (thin curves). This upper integration bound is consistent with the fitting scale of the horizontal gradients which filters out higher wavenumbers. Like the GM model, the observed convergence exceeds vorticity at low wavenumbers and is comparable at high wavenumbers. Also, the vorticity peaks at slightly higher wavenumbers than convergence in both measurements and model. This suggests that the dynamic (velocity) signal is dominated by internal waves.

3. MEDDY COMPONENT

3.1 Dynamical Aspects of the Cadiz Meddy and Hypotheses of Generation

One of the primary purposes (and accomplishments) of the Gulf of Cadiz Experiment was the detailed survey of a Meddy soon after its formation. The decay of a Meddy has recently been examined (Armi et al., 1989; Hebert et al., 1990), but the generation of a Meddy, theorized to occur by one of several different mechanisms, had not been observed.

Effort since the cruise has been placed on a thorough description of the Cadiz Meddy's characteristics and dynamical properties. The Cadiz Meddy has two distinct cores, an upper core at 1050 m depth and a second, lower core at 1350 m depth. The upper core is slightly warmer and relatively fresher than the lower core, although both are similar in properties to what is commonly referred to as the "lower" core of the Mediterranean outflow. The upper core is an isolated feature, with no connection, as seen in temperature, to the Mediterranean outflow. This core is in near solid-body rotation out to 6 km with a velocity maximum of 0.26 m s^{-1} at 9.5 km, has a core vorticity near $-0.95f$, and is in cyclo-geostrophic balance. The upper core is more energetic and axisymmetric than the lower core, which does show a connection to the outflow. The potential vorticity Q, a conservative tracer in the absence of diapycnal mixing and friction, was computed for the Meddy by

$$ Q = -(f\hat{\mathbf{k}} + \vec{\zeta}) \cdot \frac{\nabla \rho}{\rho} \approx \frac{1}{g} \left\{ (f + \zeta)N^2 - \left[f + \frac{2v}{r} \right] \left[\frac{\partial v}{\partial z} \right]^2 \right\} $$

and is shown in Figure 3.1.1. The parcels of water in the core, having near zero Q owing to low stratification and high relative vorticity, are prevented from mixing outward by the large radial gradient in Q.

We assumed that the Meddy, during its formation, entrained its two cores simultaneously, and since then no additional entrainment or mixing of the cores occurred. Thus the formation region is limited to the locations where those two water types occur in proximity. Choosing the 32.15 and the 32.30 σ_1 surfaces as the central isopycnals of the upper and lower core, and mapping the potential temperature θ_1 in the Gulf of Cadiz on those isopycnals, we found that the canyon south of Portugal was the most likely formation region (Figure 3.1.2). In this area the isobaths in the Gulf of Cadiz converge, forcing the various cores of the Mediterranean outflow to constrict over abrupt, canyon topography. Formation in this region is supported by extrapolating the position of the Meddy backward in time using its translation speed. This operation places the Meddy in the canyon region 30 days prior to our survey.
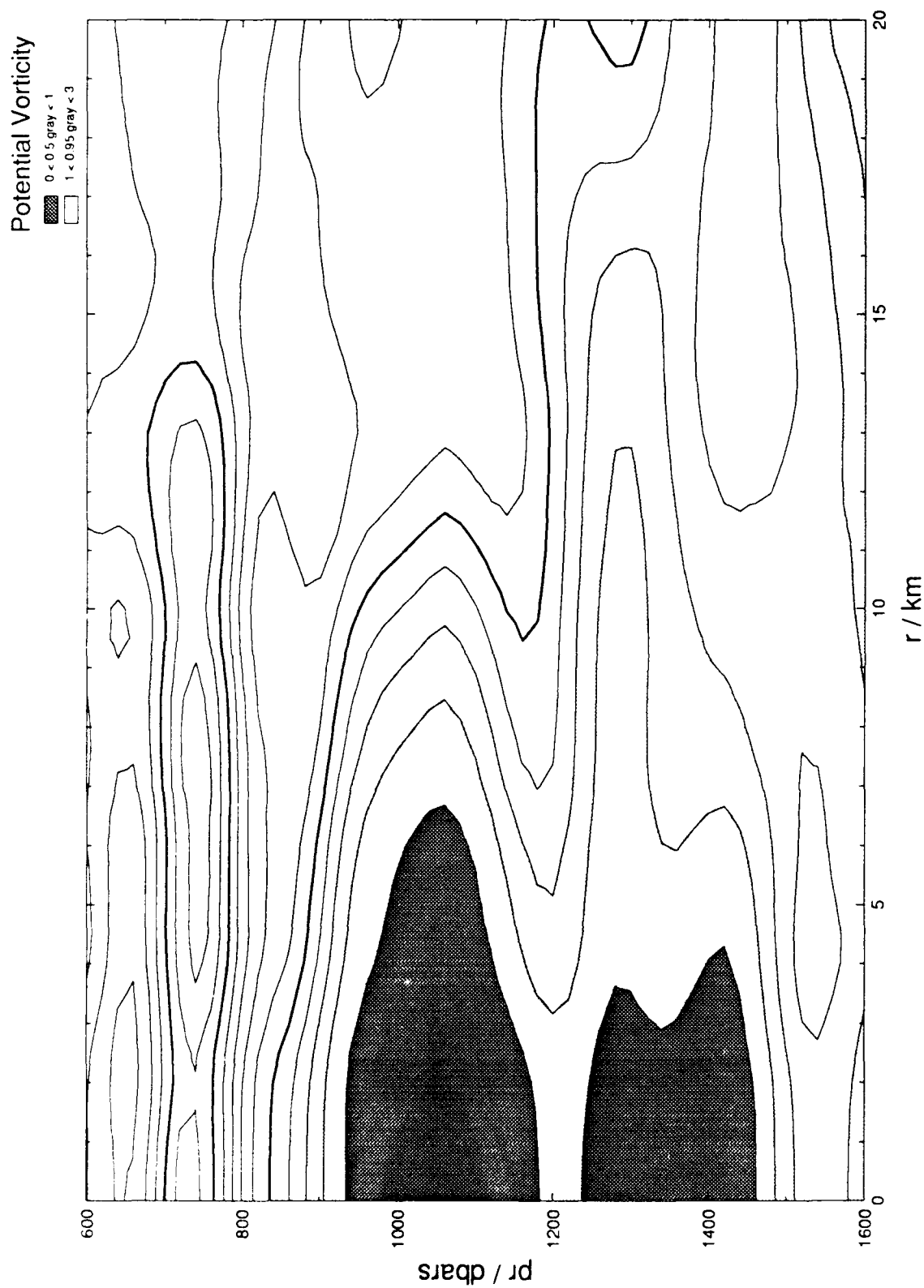
Figure 3.1.1. Contour plot of potential vorticity, Q, in the Cadiz Meddy. The contour interval is 1×10^{-11} (m s^{-1}), the dark shade denotes Q less than 1×10^{-11}, and the light shade denotes Q less than 3×10^{-11}. The values of potential vorticity are 20 to 50 times less in the center of the upper core of the Meddy than in the ambient waters.
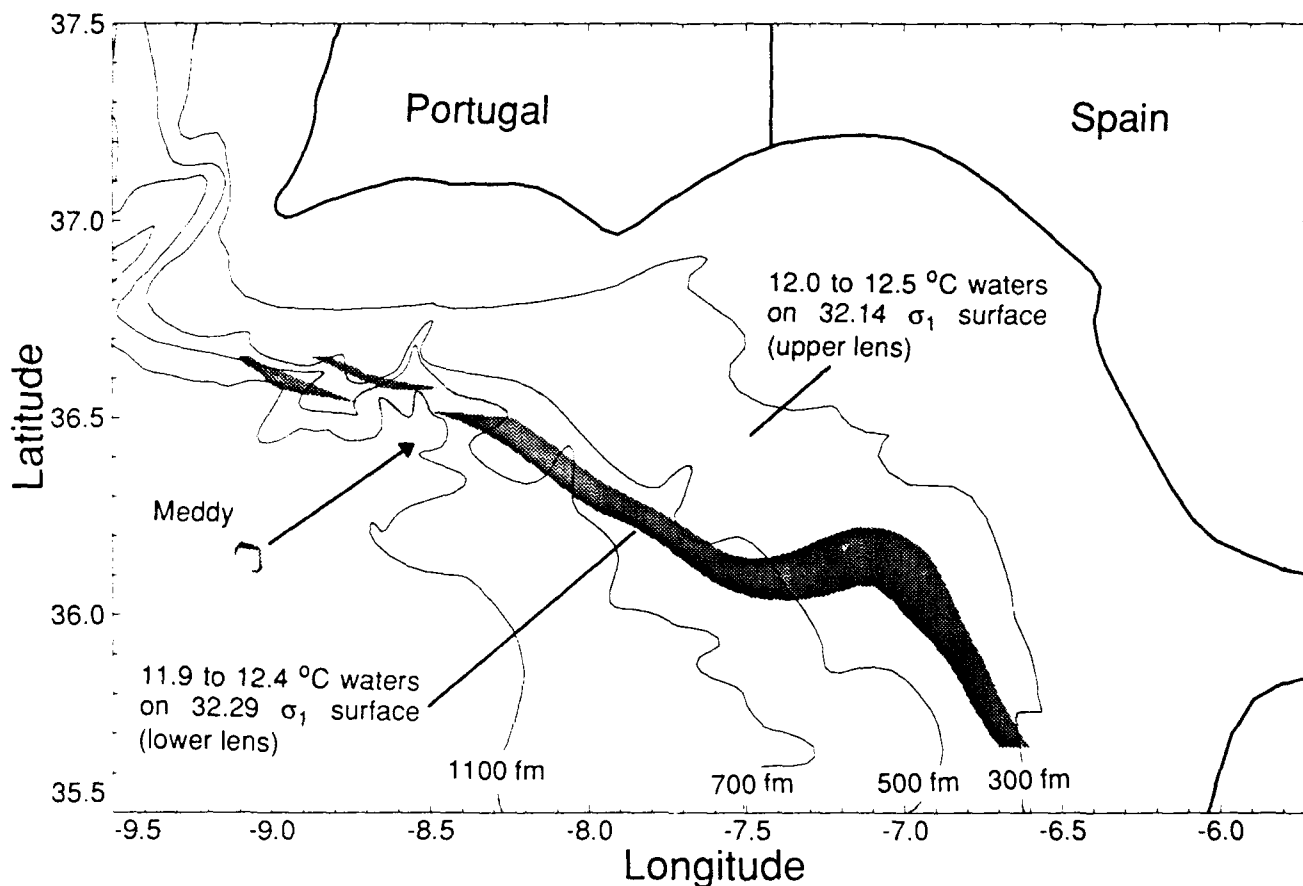
Figure 3.1.2. Chart of the Gulf of Cadiz, showing 12 to 12.5°C waters on the isopycnal corresponding to the upper Meddy core and 11.9 to 12.4°C waters on the isopycnal corresponding to the lower core. The two contours meet in the canyon region south of Portugal near 36.5°N and 8.5°W. The arrow extending northeast from the Meddy shows the backward-extrapolated path of the Meddy for the 30 days prior to the survey. The intersection of the temperature contours, the location of the extrapolated Meddy path, and the convergence of the isobaths all support the hypothesis that the canyon region south of Portugal was the formation region of the Cadiz Meddy.

The actual dynamic mechanism that generated the Meddy has been limited to three possibilities: (a) frictional torques acting to reduce the potential vorticity of the Mediterranean outflow, creating a strongly anticyclonic eddy after separation from topography (D'Asaro, 1988), (b) the instability of a buoyancy-driven boundary current (e.g., Griffiths and Linden, 1981), and (c) production of eddies by intermittent transport in an otherwise stable coastal current (Nof, 1991). The classical method of eddy generation by geostrophic adjustment is not considered to be a viable mechanism, since the Cadiz Meddy has an energy Burger number ($B_E = KE/APE$) of 4.5 and shows little evidence of having been gravitationally compressed. Eddies generated by geostrophic adjustment having such a high B_E are compressed by a factor of 3 or greater (McWilliams, 1988).

Section 3.1 was contributed by Mark D. Prater,
Applied Physics Laboratory, University of Washington.

4. MEDITERRANEAN OUTFLOW COMPONENT

4.1 Large-Scale Structure of the Mediterranean Outflow

The Gulf of Cadiz Expedition in September 1988 aboard the R/V *Oceanus* partly focused on the dynamics and large-scale structure of the Mediterranean outflow where it descends into the Gulf of Cadiz. Numerous closely spaced salinity, temperature, and current profiles (acquired along sections A through I in Figure 1.1) gave us a greatly improved picture of the overflow, in particular a detailed picture of the mixing and dynamics within the first 40 km, or 500 m of descent.

The overall structure of the outflow is similar to that described in the historical literature such as Heezen and Johnson (1969) or Madelain (1970), confirming the fairly steady nature of the flow over decades. The outflow lies entirely on the continental slope during its initial descent into the Gulf of Cadiz, where it mixes with fresh North Atlantic water, reducing its salinity anomaly and increasing its transport. During the first 100 km of descent, the overflow transport doubles from 0.85 Sv to 1.9 Sv, and the overflow broadens from 10 km to 90 km. Cross-stream variations in the overflow T/S properties increase as the flow spreads. Slightly differentiated water types exit the strait, with the saltiest, coldest outflowing water to the south and slightly fresher and warmer outflow to the north (Figure 4.1.1). Since the northern, near-shelf flow is higher in the water column, it mixes with warmer North Atlantic water than the deeper offshore flow. What begins as less than a $0.5°C$ cross-stream variation in water types in the strait becomes more than a $2°C$ variation as the flow spreads within the first 100 km (Figure 4.1.2). The flow eventually settles along two preferred isopycnals: 27.5 and 27.8 (Zenk 1975).

Our hydrographic data show a maximum core salinity of 38.4 psu at the strait and a decrease of 0.6 psu in 40 km. Combining hydrographic data with the current measurements suggests a much more intense mixing process. The velocity-weighted salinity of the outflow begins with a salinity of 37.7 psu near the strait and decreases over 1 psu within the first 40 km. The difference between the core salinity values and the velocity-weighted salinities is due mostly to the stratified nature of the outflow. Core salinity values, which are located within 10 m of the bottom, do not accurately reflect the average properties of the 100 m thick outflow. The overflow becomes neutrally buoyant near Cape St. Vincent, over 300 km from the strait where the core salinity is 36.6 psu. Since the velocity-weighted salinity has already attained a value close to this only 40 km from the strait, most of the mixing has taken place within the first 40 km.

The criterion for Kelvin-Helmholtz instability is that the gradient Richardson number is less than 1/4. We found low gradient Richardson numbers in the well-mixed outflowing layer where the stratification is very weak and also near the interface between outflowing water and the return circulation above. At the interface the stratification is very high but the velocity shear is so large it could overcome the stability of the buoyancy forces. These low gradient Richardson numbers suggest the flow is unstable to
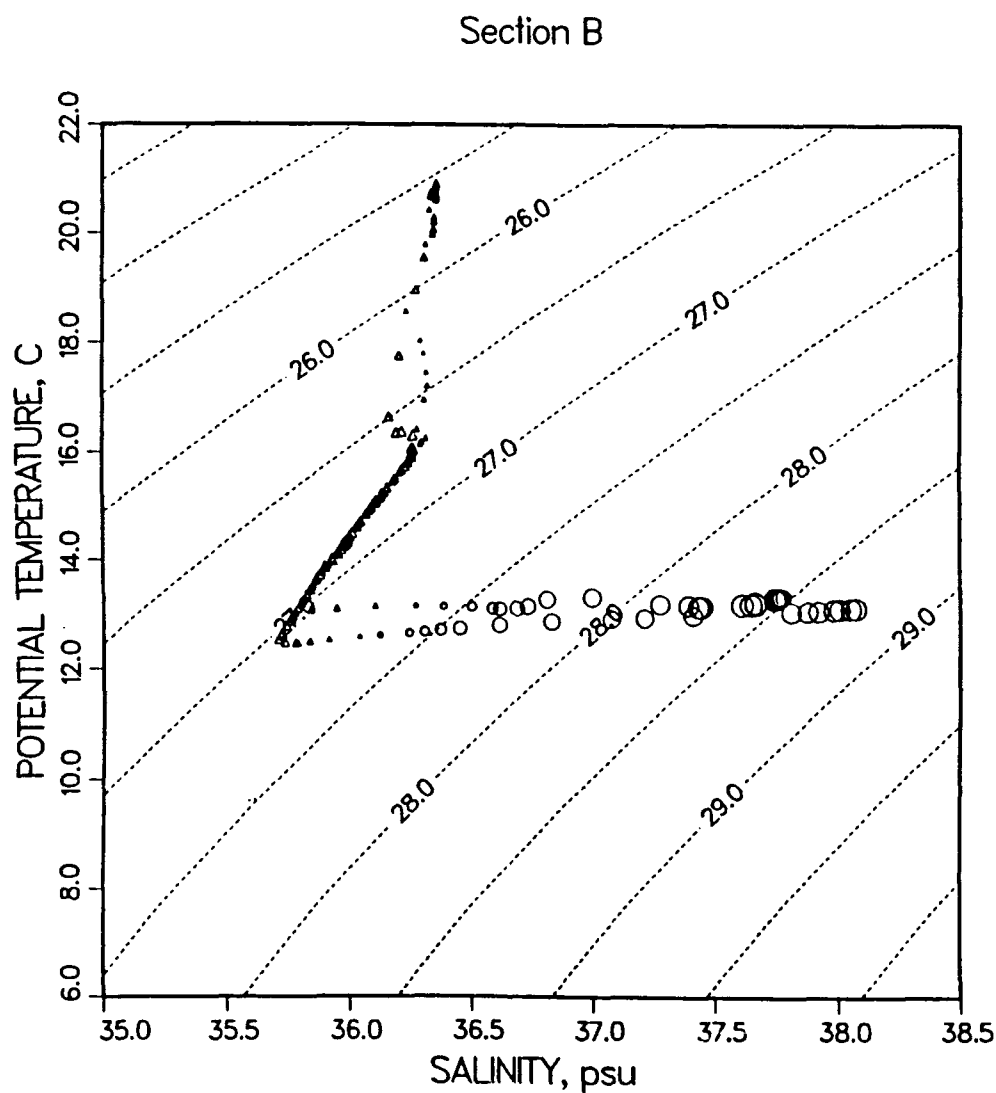
Section B

Figure 4.1.1. Potential temperature versus salinity for Section B. Triangles represent eastward moving water as determined from the XCPs. Circles represent westward moving flow. The symbols are scaled by the flow speed and plotted for every 4 m of data. Dashed lines show contours of potential density. This figure shows rapidly moving salty Mediterranean water moving to the west. Only two stations across this section indicated the presence of Mediterranean outflow. The northern station is very slightly warmer and fresher than the southern station.

Section F
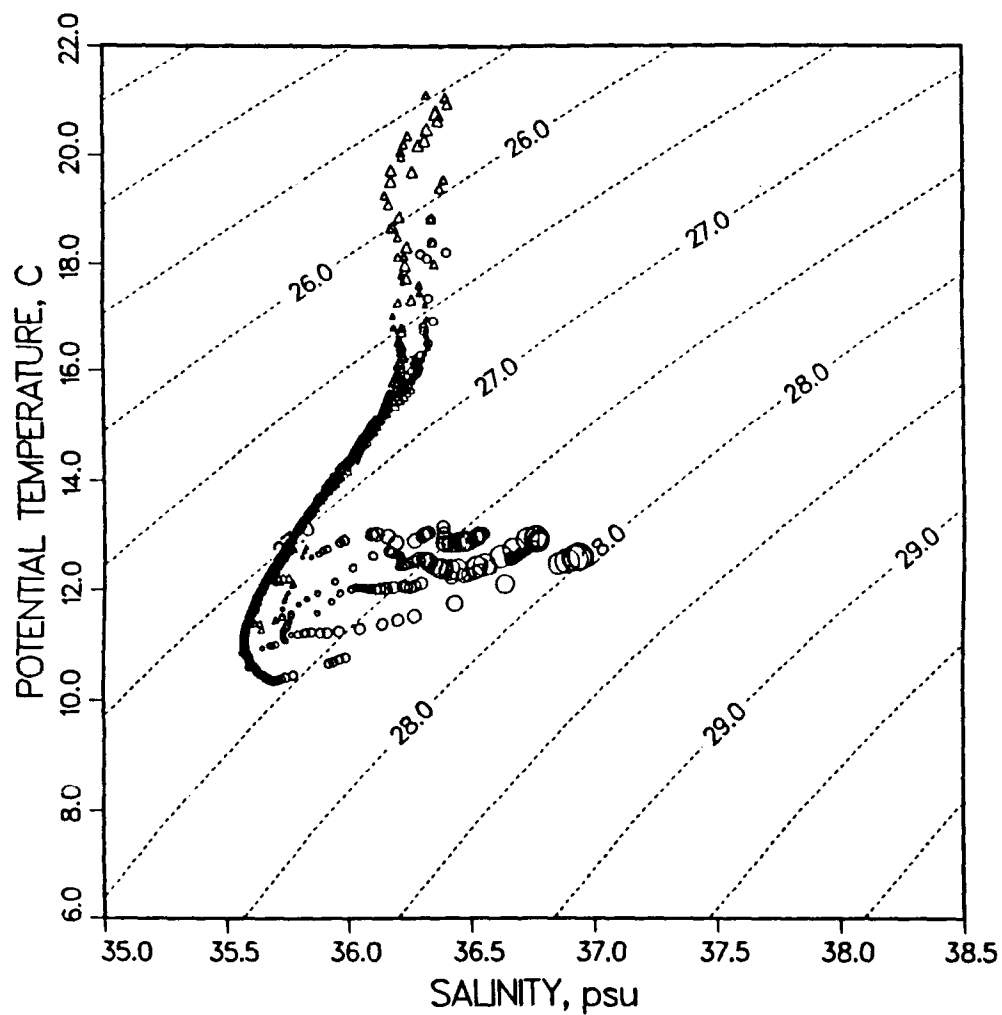
Figure 4.1.2. Potential temperature versus salinity for Section F. At section F, 80 km downstream of section B, there is more than a 2°C horizontal variation in outflow temperature. The northern stations have become warmer as the outflow mixes with warm North Atlantic water.

Kelvin-Helmholtz instability and could be mixing through this mechanism. Bulk Richardson numbers or, equivalently, bulk Froude numbers suggest the same thing (Figure 4.1.3). Supercritical Froude numbers, Fr > 1, were found near the strait coincident with the vigorous mixing observed through the salinity and transport calculations. Farther from the strait, lower bulk Froude numbers were observed in regions in which we believe less entrainment is taking place (Figure 4.1.4).

CTD76, XCP45, SECTION C
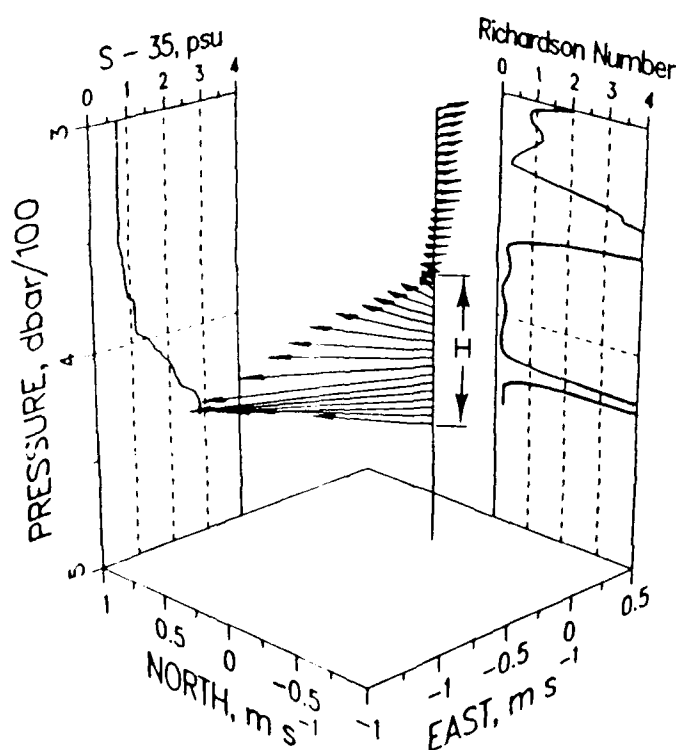
Bulk Richardson Number:

$$Ri_b = \frac{g'H}{(\Delta U)^2}$$

Froude Number:

$$F = \frac{\Delta U}{(g'H)^{1/2}}$$

$Ri_b \approx 0.67$

$F \approx 1.2$

Figure 4.1.3. Three-dimensional velocity vector diagram for XCP 45/CTD 76. The XCP velocity versus depth is plotted for every 4 m of data. The corresponding salinity anomaly and gradient Richardson number are also plotted. This figure shows salty Mediterranean water moving toward the NW with low gradient Richardson numbers. Low gradient Richardson numbers are also found in the interface and the well-mixed bottom layer. This figure demonstrates how bulk Richardson numbers and Froude numbers are calculated. The average temperature and salinity of the overflow were calculated using the velocity-weighted properties, and the change in shear was calculated from vertically averaging the velocity. The bulk Froude number for this profile was supercritical.

Gulf of Cadiz
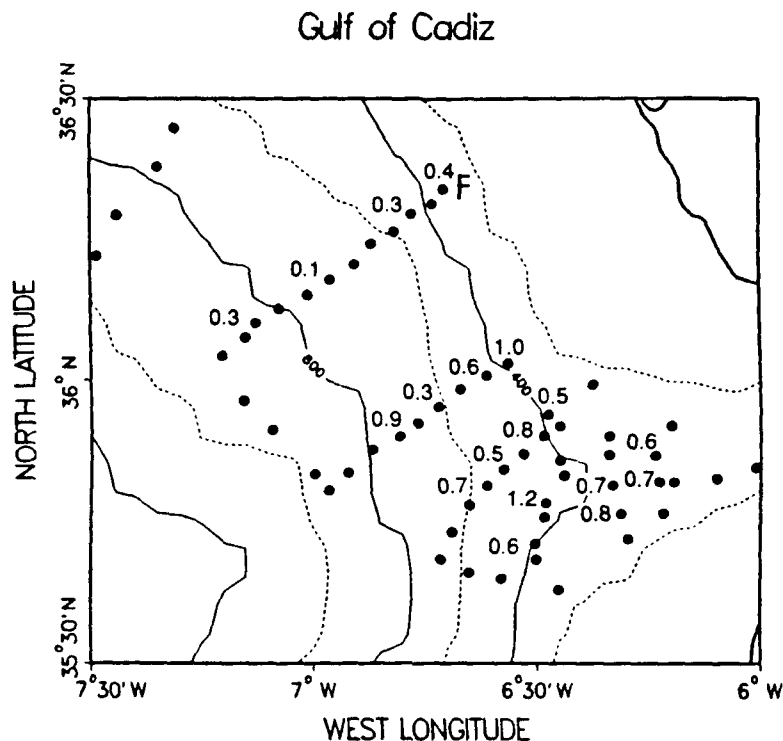
Figure 4.1.4. Station map showing selected bulk Froude number estimates. Near the strait, the bulk Froude numbers were higher than they were at Section F, where we believe less mixing is taking place.

Near the strait, advection, dissipation, and the Coriolis force all make important contributions to the dynamics of the flow. Farther downstream, the flow becomes a damped geostrophic current. After the flow exits the strait, it takes a right-hand turn into the Gulf of Cadiz. This deflection of the current represents a nearly inertial turn in the flow, where the advection terms are the same order of magnitude as the pressure gradient. Examination of the downstream momentum flux divergence suggests an average stress of 2 Pa retarding the flow within the first 100 km of descent. Near the strait, the stress may be as high as 5 Pa, while farther downstream the stress decreases to 1 Pa (Figure 4.1.5). Most of the potential energy released from the flow is due to the descent of the current down the continental slope. This decrease in potential energy is dissipated instead of increasing the kinetic energy of the mean flow.

Section 4.1 was contributed by Molly O. Baringer,
Woods Hole Oceanographic Institution.
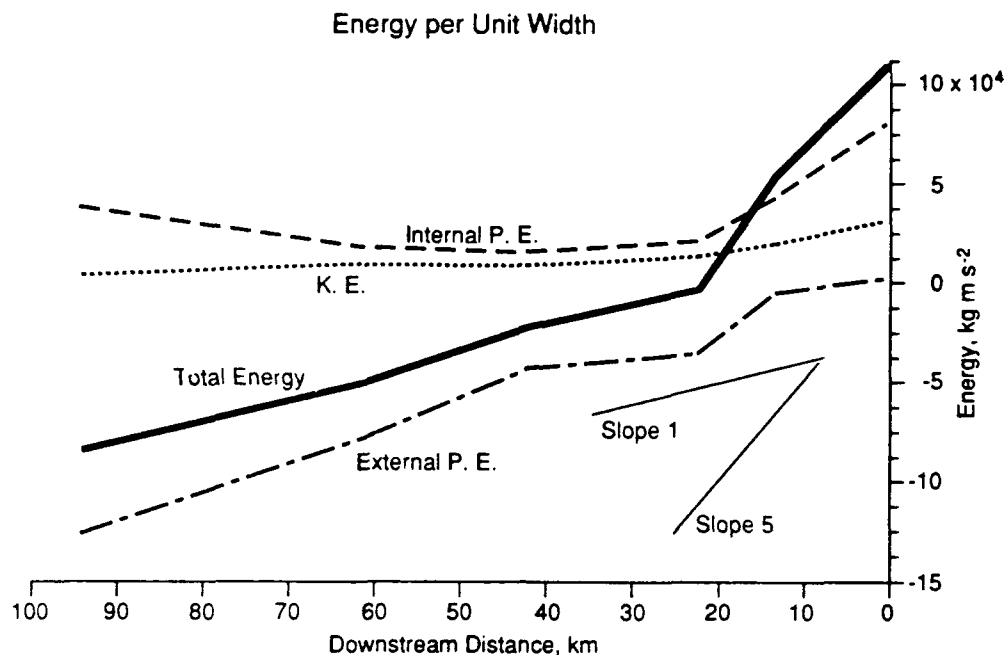
Figure 4.1.5. Energy balance terms normalized by the width of the outflow. The external potential energy (dot-dashed line) decreases as the outflow slides down the continental slope. The changes in the internal potential energy (dashed line) mostly reflect the changes in outflow height. The kinetic energy (dotted line) is an order of magnitude less than the potential energy. The potential energy is not converted into kinetic energy. This loss of total energy (solid line) suggests the presence of large stresses retarding the flow. To obtain stress estimates from the horizontally integrated momentum equation, we must divide by the width of the outflow. The total stress is the downstream divergence of the total energy (solid line). This calculation suggests a total stress of 5 Pa retarding the outflow within the first 25 km of Section A. Farther downstream the stress decreases to 1 Pa.

4.2 Modeling Oceanic Overflows

There are four major overflows that supply dense waters to the thermocline or abyssal North Atlantic (Figure 4.2.1). In order of increasing density of the final product, these are (a) the Mediterranean overflow, which injects warm salty water into the North Atlantic thermocline, (b) the overflows across the Iceland-Scotland Ridge, which supply warm and salty deep water to the eastern North Atlantic, (c) the Denmark Strait overflow, which supplies bottom water to the northern North Atlantic, and (d) the Weddell Sea overflow, which supplies cold fresh bottom water to the Weddell Sea that goes on to become Antarctic Bottom Water. These overflows all begin in marginal seas and then spill over a ridge or sill before they enter the North Atlantic. Along the way they entrain oceanic waters having quite different properties and thus end up with final properties (T, S, and density) that are quite different from those found near the sill or strait connecting with the marginal sea.

We have developed a simple model of overflows that we are using to try to understand why some overflows produce bottom water (the second two mentioned above), while others form interflows in the thermocline. This is especially intriguing in the case of the Mediterranean and the Denmark Strait overflows since the Mediterranean overflow begins with a very high initial density.

Our model suggests that the principal external variables that determine the intensity of mixing are the bottom slope (large slopes cause stronger currents and more mixing), the earth's rotation (smaller rotation gives larger geostrophic currents), and the initial transport (small initial transport leads to thinner overflow plumes which are more susceptible to mixing). A greatly simplified model including just these variables can be used to find the explicit dependence of mixing on the geostrophic Froude number and the initial Froude number (Figure 4.2.2). Given an estimate of the geostrophic Froude number, we can then use this result to estimate what fraction of the initial density difference will be lost due to mixing, and we have done this for each of the overflows shown schematically in Figure 4.2.1. In Figure 4.2.3, we plot the density lost against a density ratio that measures the stratification between the initial overflow and the bottom water. If the density loss is greater than this density ratio, then the overflow will form an interflow (upper left half of the diagram); otherwise it will reach the bottom. The Mediterranean overflow is solidly within the interflow half, whereas the Denmark Strait case is on the other side, though not by a great deal. In any event, we can see the Mediterranean case has both a moderately large geostrophic Froude number and fairly strongly stratified ambient water, which both contribute to making an interflow.

Section 4.2 was contributed by James F. Price,
Woods Hole Oceanographic Institution.

Oceanic Overflows

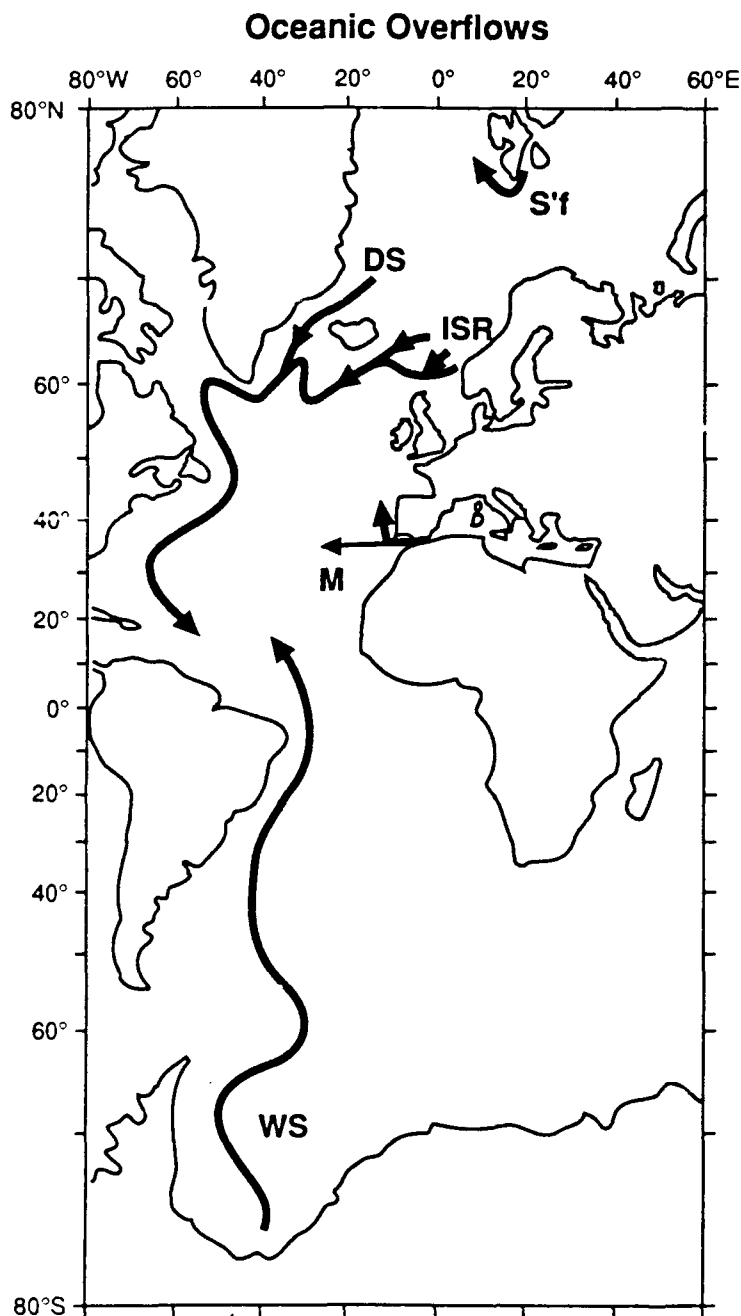**DS** - Overflow of Arctic Intermediate Water through Denmark Strait. Forms bottom water in northern North Atlantic and contributes to the Deep Western Boundary Current.

	Before Overflow	After Overflow	
θ	0.5°C	1.0–2.0°C	
S	34.92 psu	34.90 psu	
σ_θ	28.02	27.92	$\Delta\sigma_\theta = 0.10$

ISR - Overflow of Norwegian Sea Deep Water through Faeroe Bank Channel and across the Iceland-Scotland Ridge. Forms bottom water in northeastern North Atlantic and contributes to the Deep Western Boundary Current.

	Before Overflow	After Overflow	
θ	0.0°C	2.5–3.5°C	
S	34.92 psu	35.00 psu	
σ_θ	28.05	27.90	$\Delta\sigma_\theta = 0.15$

M - Overflow of Levantine Intermediate Water through the Strait of Gibraltar. Forms a warm salinity maximum within the North Atlantic thermocline.

	Before Overflow	After Overflow	
θ	13.5.0°C	12.0°C	
S	38.2 psu	36.4 psu	
σ_θ	28.78	27.69	$\Delta\sigma_\theta = 1.1$

WS - Overflow of Ice Shelf Water from Filchner Depression which forms Antarctic Bottom Water. When combined with other Antarctic overflows, this water covers most of the abyssal Atlantic and world ocean.

	Before Overflow	After Overflow	
θ	−1.9°C	−0.5°C	
S	34.68 psu	34.65 psu	
σ_θ	27.94	27.86	$\Delta\sigma_\theta = 0.08$

Figure 4.2.1. Schematic of the major overflows that contribute to deep and intermediate waters in the North Atlantic.
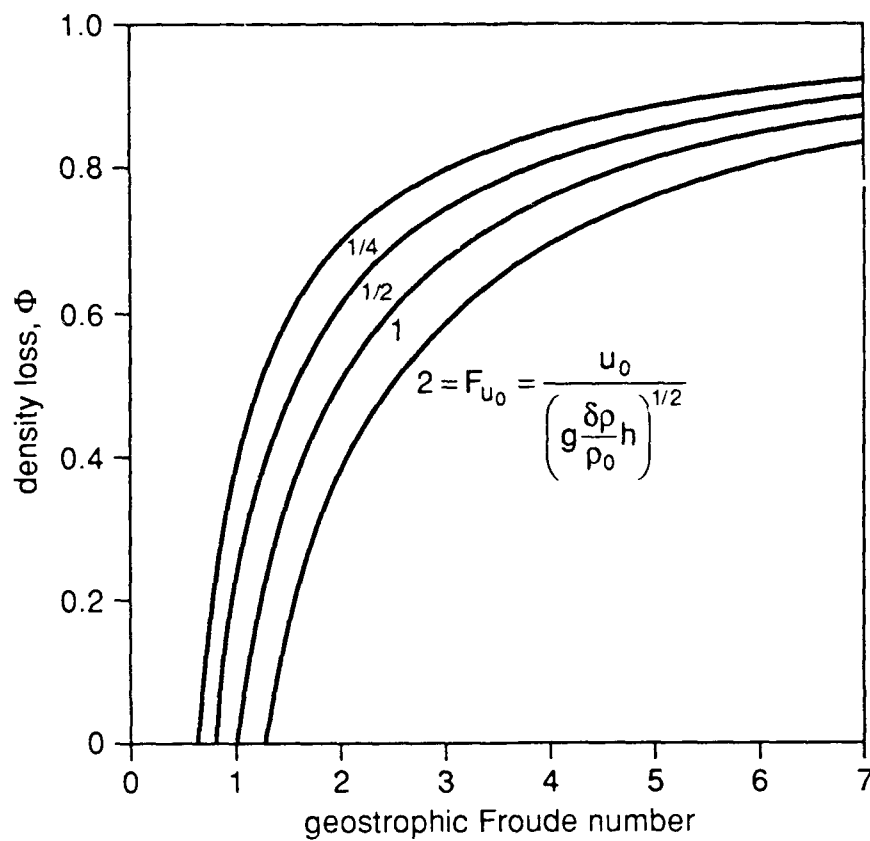
Figure 4.2.2. Fractional density loss of the overflow as a function of the geostrophic and initial Froude numbers. Each curve represents a different initial Froude number.
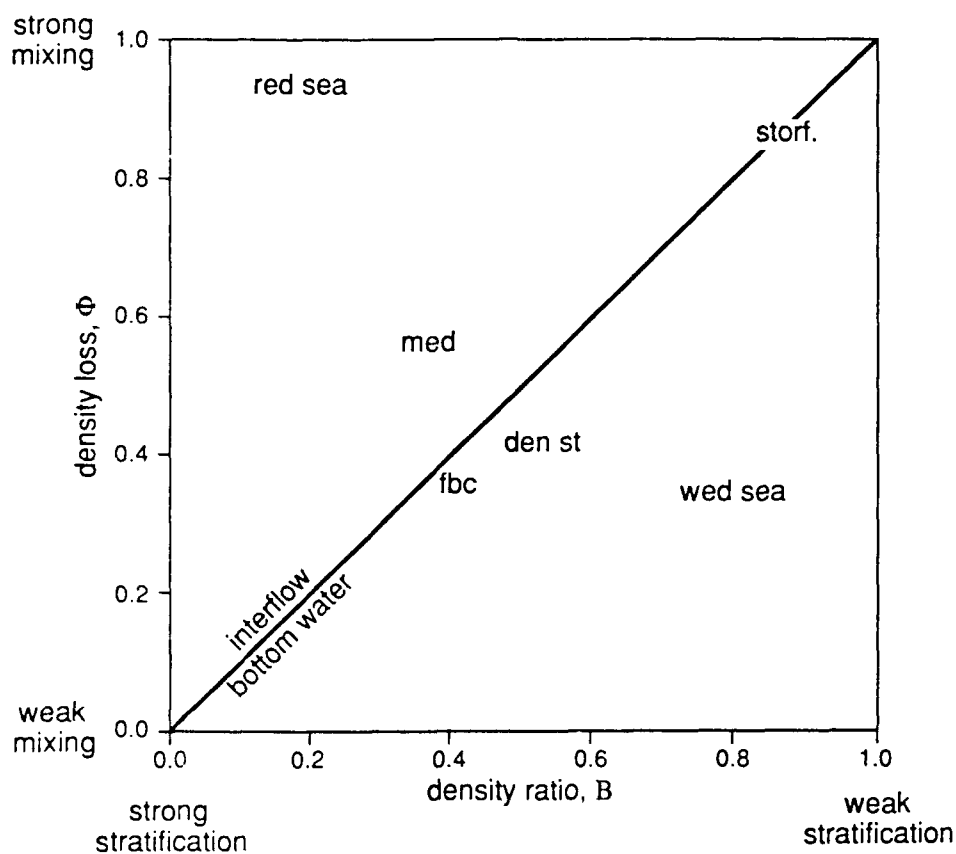
Figure 4.2.3. Density loss versus density ratio for the overflows of Figure 4.2.1. Cases that fall in the upper left quadrant are expected to make interflows, whereas those in the lower right are likely to make bottom water. ("storf." = Storfjorden Fjord, "den st" = Denmark Strait; "fbc" = Faeroe Bank Channel)

4.3 Bottom Stress

The stresses imparted to the Mediterranean water plume from underneath are produced by viscous bottom stress and form drag. The latter contribution has been reported by other investigators (Chriss and Caldwell, 1982, on a shelf; Gust and Weatherly, 1985, for the deep ocean) and most certainly is large here because of the bottom roughness (Heezen and Johnson, 1969). The dissipation measurements of the XDP (expendable dissipation profiler) determine viscous stress whereas the profile observations of the XCP are interpreted in terms of form drag. This experiment allows us to compare viscous versus form drag stresses.

The viscous bottom stress, τ_B, has been estimated using high-resolution (0.1 m) profiles of the rate of dissipation of kinetic energy, ϵ, collected with XDPs. For a steady and horizontally homogeneous bottom boundary layer, ϵ decreases with increasing height, z, above the bottom as

$$\epsilon = \frac{u_*^3}{\kappa z},$$
(1)

where $u_* = (\tau_B/\rho)^{1/2}$ is the friction velocity and $\kappa = 0.4$ is von Karman's constant (Dewey and Crawford, 1988). Nearly all profiles conformed to the functional form of (1). The spatial distribution of τ_B (Figure 4.3.1) was coincident with the axis of maximum flow of Mediterranean water. The stress increased downstream from site 3 and reached a maximum of 2 Pa ($u_* = 0.044$ m s^{-1}) between survey lines C and D (see Figure 1.1 for line locations). This maximum occurred where the plume veered north by 90°. The bottom stress decreases farther downstream, but the sampling was inadequate for a quantitative description of this trend.

A regression of u_* against the maximum speed of the plume gives a drag coefficient of $C_D = 0.9 \times 10^{-3}$ (Figure 4.3.2), while a regression against the mean speed of the plume gives $C_D = 2.6 \times 10^{-3}$ (Figure 4.3.3). Drag coefficients are traditionally based on the speed at 1 m above the bottom, but such an estimate is not available for the Mediterranean plume. However, it is clear that the derived drag coefficients considerably exceed the estimate of 0.6×10^{-3} by Dewey and Crawford (1988) using a similar technique for a tidal flow over the continental shelf.

Using the equation for the conservation of mean kinetic energy and integrating it over the height, H, of the plume, it can be shown that

$$H \frac{<\epsilon>}{<u>}$$
(2)

is a reasonably good estimate of the total stress, where $<\ >$ indicates an average over the height of the plume. This estimate of the total stress is typically twice the bottom stress, τ_B, and ranges from 1 to 5 Pa near the axis of the plume (Table 4.3.1).

The use of XCPs to determine bottom stress is a new endeavor, and this experiment provides an opportunity to examine the method and compare the results with the viscous
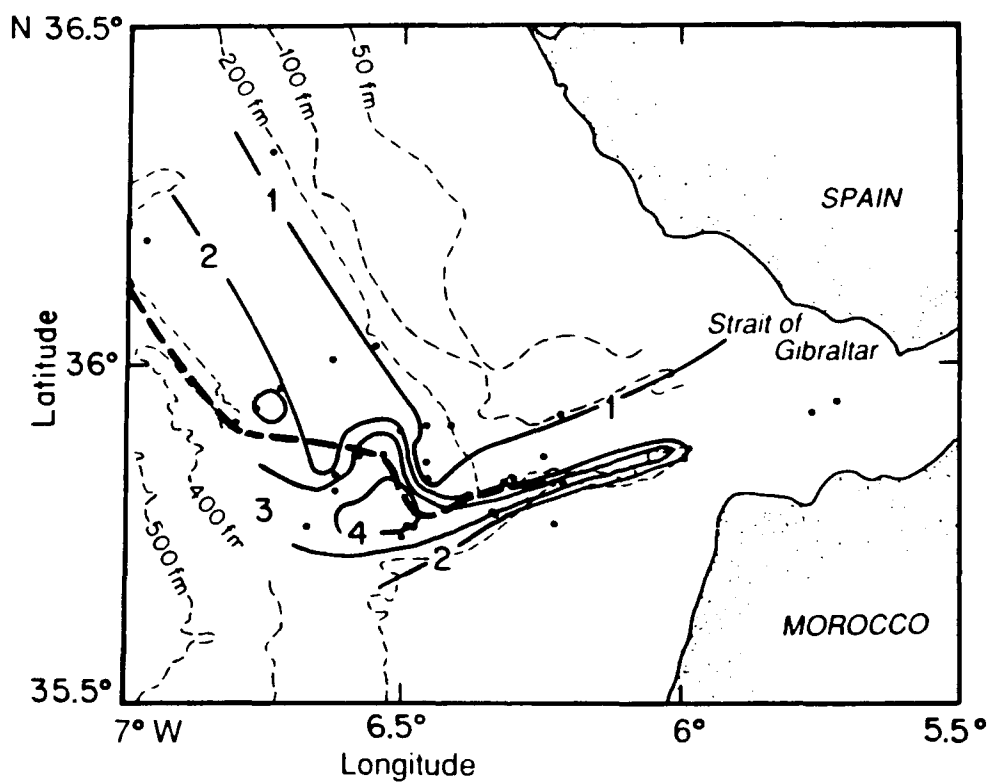
Figure 4.3.1. Spatial distribution of τ_B.
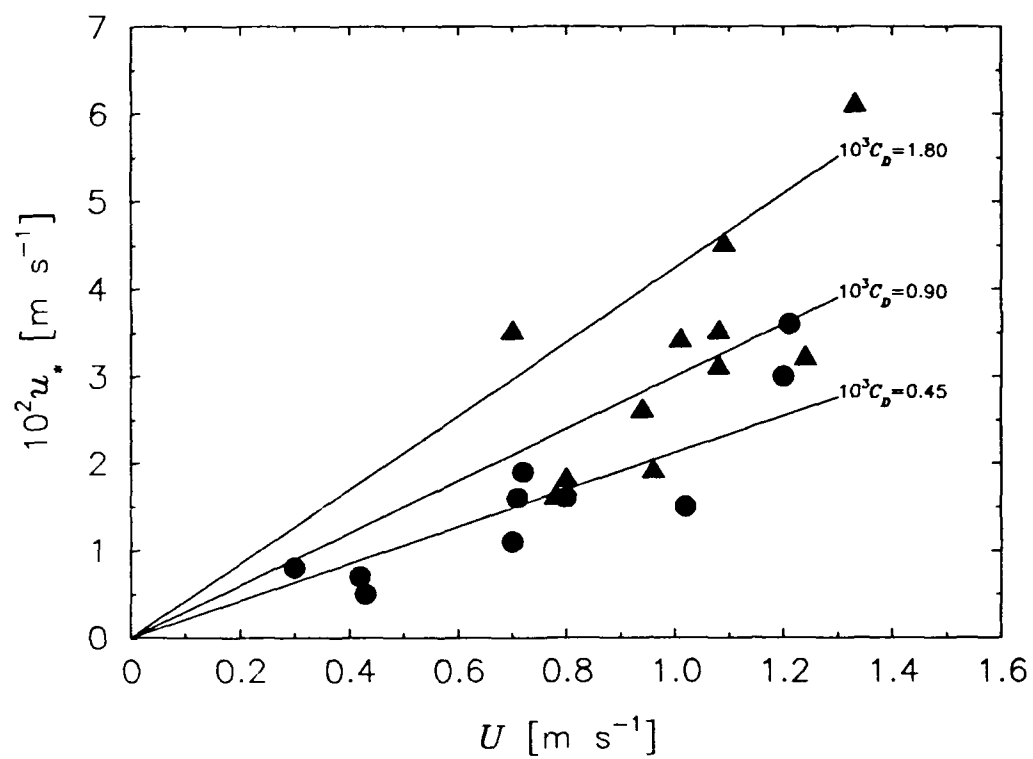
Figure 4.3.2. Regression of u_* against the maximum speed of the Mediterranean outflow plume.
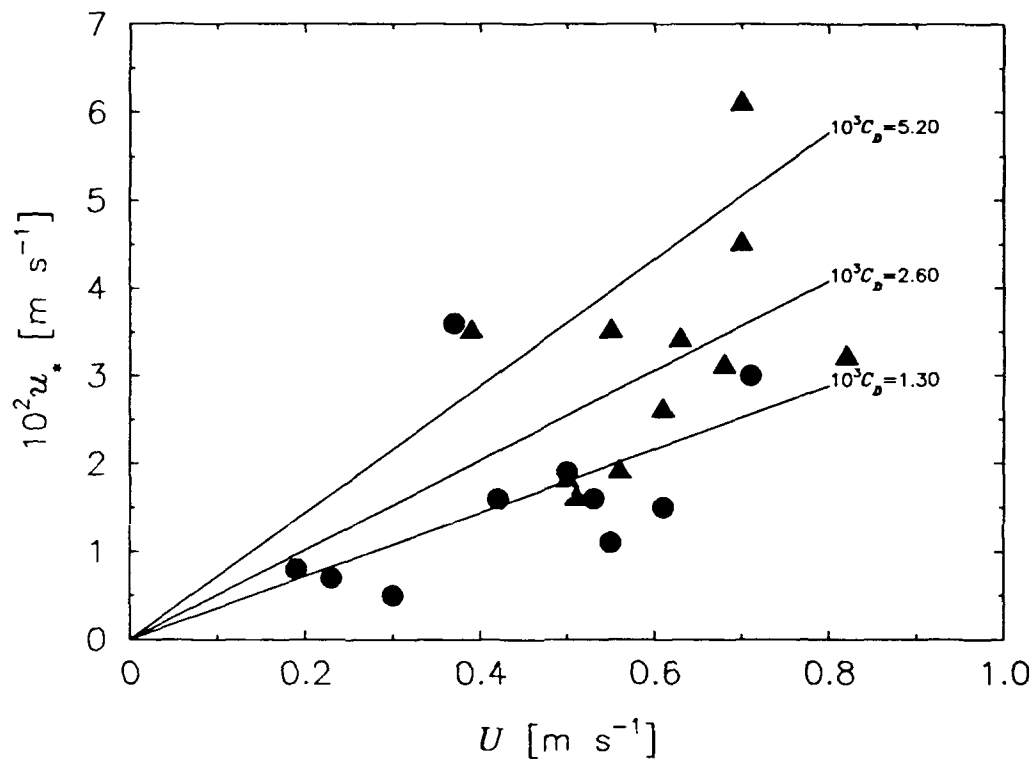
Figure 4.3.3. Regression of u_* against the mean speed of the Mediterranean outflow.

Table 4.3.1 Mediterranean outflow stress estimates.

XCP	$\langle U \rangle$ [m s^{-1}]	H [m]	XDP	$10^3 \langle \epsilon \rangle$ [W m^{-3}]	$H\dfrac{\langle \epsilon \rangle}{\langle U \rangle}$ [Pa]	ρu_*^2 [Pa]	Site	Line	Comments
2527	0.54	176	1040	0.89	0.29	0.26	1	A	
2530	0.51	156	701	3.8	1.1	0.54	1	A	
2530	0.51	156	803	1.4	0.4	0.33	1	A	
2523	0.77	142	801	7.2	1.3	1.0	2		
2577	0.42	144	1072	0.83	0.28	NH	2		
2528	0.70	88	1035	11.3	1.4	0.64	4	B	
2531	0.71	82	709	50.	5.8	3.8	4	B	
2529	0.58	112	808	9.8	1.9	0.37	5	C	
2532	0.69	108	707	8.0	1.2	2.1	5	C	
2538	0.61	146	1034	0.74	0.18	0.15		A	
2541	0.54	114	1043	0.60	0.12	0.12		B	
2579	0.50	108	1059	7.8	1.7	0.37	(2541)	B	
2544	0.63	108	704	3.9	0.66	1.2		C	
2556	0.84	100	804	125.	14.8	1.1	(2544)	C	Bang
2580	0.71	116	1060	19.	3.2	0.92	(2544)	C	
2551	0.61	94	813	16.	2.5	1.26		D	Noisy
2562	0.49	88	828	20.	3.5	0.26		E	
2563	0.61	164	711	8.0	2.2	0.69		E	
2578	0.56	150	1055	7.2	1.9	0.26		A	

stress estimates obtained from the XDP. The procedure is to fit the observed velocity profile to a log function. The mean velocity profile is expected to have the following form:

$$u = \frac{u_*}{\kappa} \ln(z/z_o) , \qquad (3)$$

where u_* and κ were defined earlier and z_o is a bottom roughness scale. The u_* determined by (1) and (3) are not necessarily the same. They will differ for a number of reasons, including the influence of form drag, which is exhibited only in the profile used in (3).

One of the first questions we asked about using the profile method on these data was the reproducibility of u_* over a time series of profiles. There were two sites that were repeatedly sampled. Site 5, also denoted as station 4 on section C, was sampled a number of times. Four drops were made here early in the experiment to determine if there were strong tidal fluctuations, and two more were taken later on section C and section I. The observations, spanning 6.5 days, are shown in Figure 4.3.4. The upper two panels show the filtered, total water column profile. The third panel shows the downstream velocity component at the finest vertical resolution possible (a value for every XCP rotation, about 0.3 m) plotted as a function of the log of height above the bottom. The flow estimates are fitted to a linear function by a least-squares method to obtain the stress estimates, shown in the bottom panel expressed both as stress (τ) and friction velocity (u_*). These estimates are quite steady: $\tau = 5.2 \pm 1.9$ Pa and $u_* = 7.0 \pm 1.2$ cm s^{-1}.

It was expected that the u_* values obtained from the XCP and XDP observations would be different. Dewey and Crawford (1988) found that u_* values obtained from fits to velocity log layers were consistently 4.5 cm s^{-1} larger than those determined from dissipation profiles. We observe a similar result from the fits to XCP profiles and the XDP dissipation profiles. The two instruments were often dropped several minutes and several hundred meters apart. The comparison, shown in Figure 4.3.5, has a slope of 3.2.

As shown in Figure 4.3.6, there was a large change in bottom stress as the plume accelerated between sections A and C. In section A the plume is thicker and slower than in section C. Bottom stress τ increases by about an order of magnitude in the maximum salinity part of the plume.

A summary of the behavior of bottom stress and friction velocity as a function of downstream distance is shown in Figure 4.3.7. The sections have been aligned so that the position of the salinity maximum is taken as the origin. Most of the action occurs around sections C and D in the highly saline water. After section D, the plume seems to spread laterally and slowly, probably forming the two distinct cores that are characteristic of the Mediterranean outflow.

Section 4.3 was contributed by Rolf Lueck, University of Victoria, and Thomas B. Sanford, Applied Physics Laboratory, University of Washington.

Cadiz Site 5 / C4
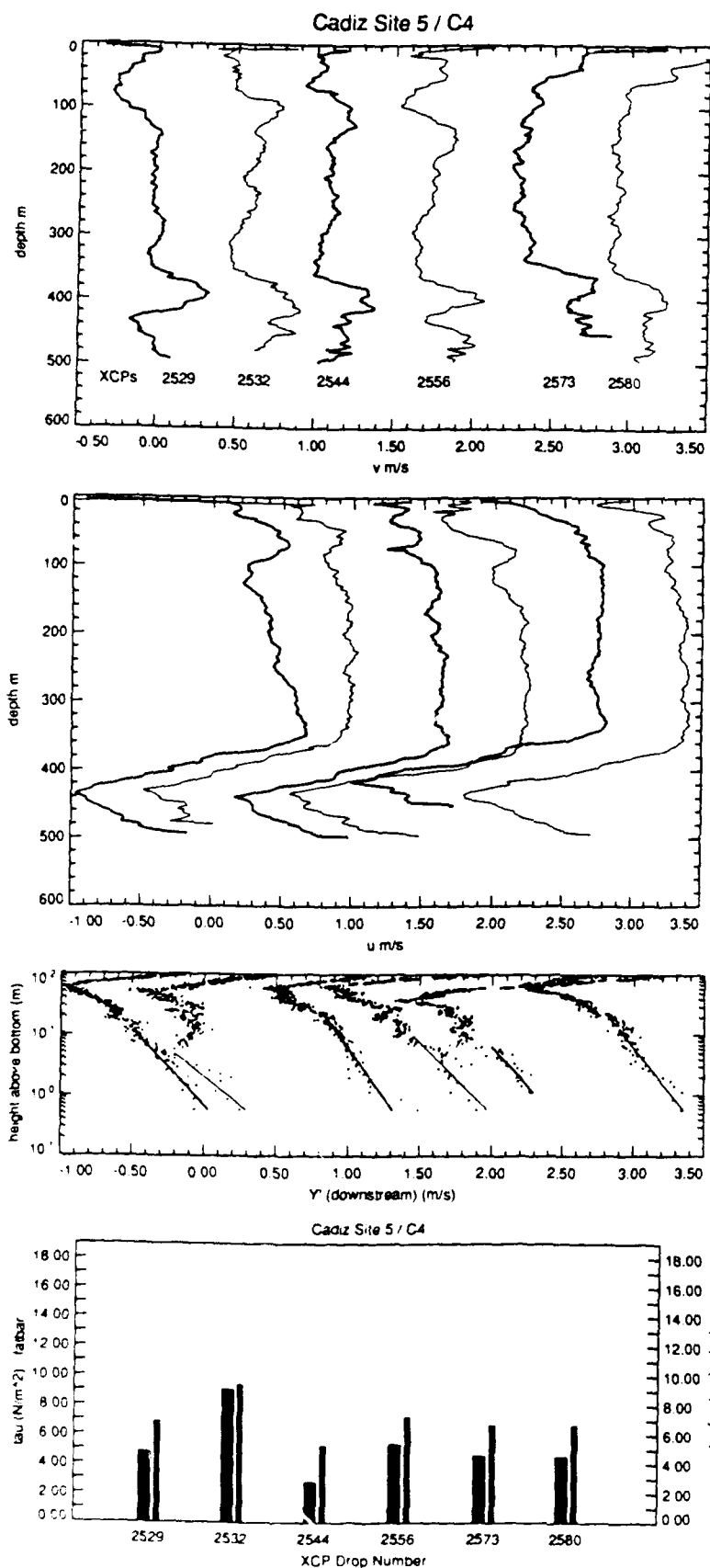
Figure 4.3.4.

Velocity profiles at site 5 (a.k.a. section C station 4) expressed in magnetic north (v) and east (u) velocity components (top two panels) for the whole water column and the downstream component expressed as a function of height above the bottom (third panel). Least-square fits are shown for the lower 10 m of each downstream-component profile versus log height off the bottom. The lowest panel displays the calculated bottom stress τ and friction velocity u_*.

Figure 4.3.5. Comparison of friction velocities derived from XDP dissipation observations and those derived from XCP measurements. The slope of the regression is 0.32.
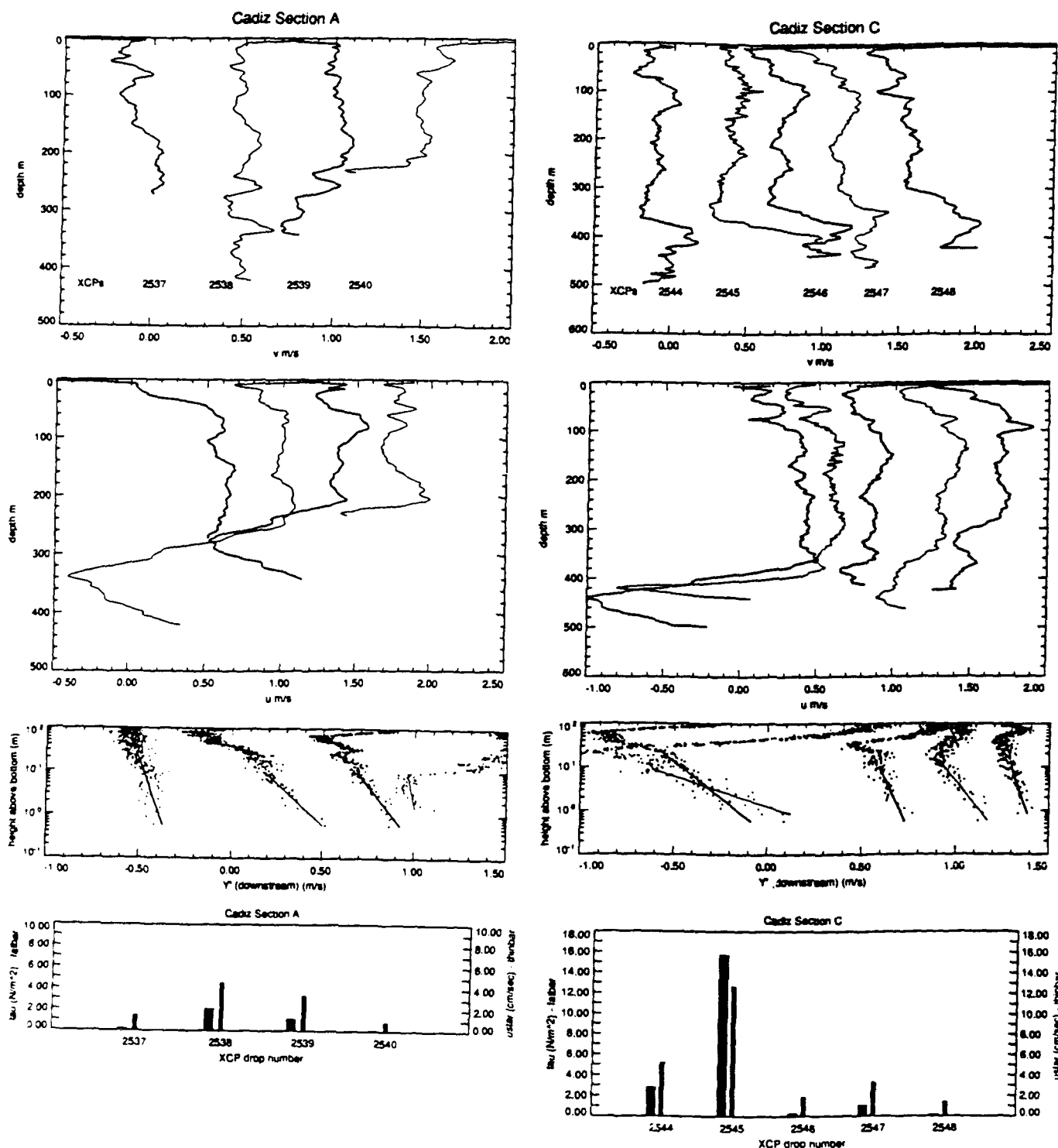
Figure 4.3.6. Same display as described in Figure 4.3.4, but for sections A and C. Note deepening, thinning, and acceleration of the flow between these sections.
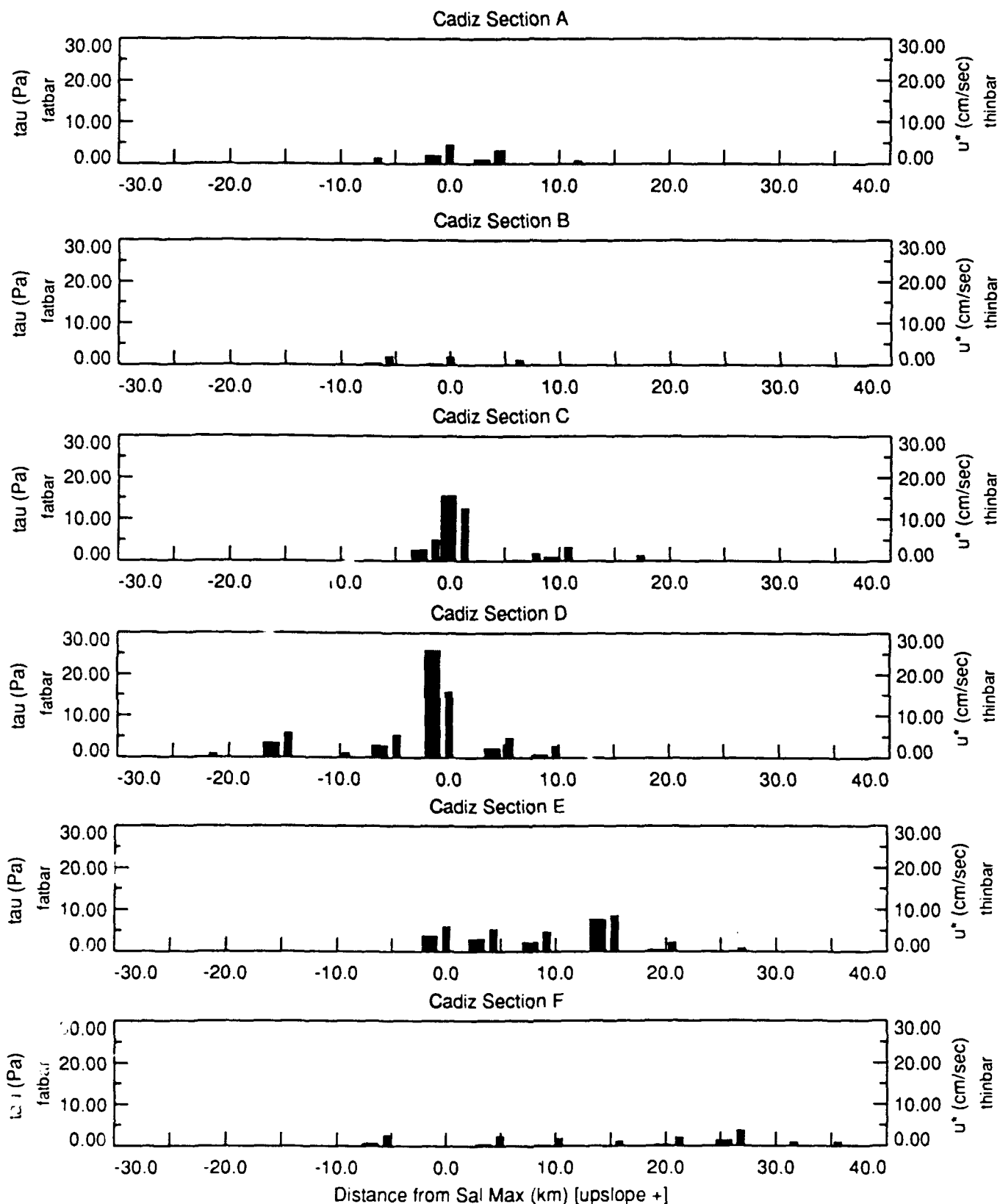
Figure 4.3.7. Summary of bottom stress observations from XCP profiles for sections A through F. Note peaking of bottom stress around sections C and D and the broadening of strongly stressed flow along section E. Origins of cross-stream coordinates are the positions of the maximum salinity found on each section.

4.4 Comparison of Velocities Derived from XCP and CTD Sections

CTD and Expendable Current Profiler (XCP) data were collected across the Mediterranean outflow in the Gulf of Cadiz and in coastal waters off Portugal during the *Oceanus* 202 cruise in September 1988. For each section, velocities directly measured by XCPs are compared with geostrophic velocities calculated from the CTD data. The XCP velocities are determined by measuring the electric fields induced by the ocean's motion through the earth's magnetic field. We calculated the component of the XCP velocities normal to each section for comparison with the geostrophic currents.

Since both velocity-measurement techniques are accurate only to within a constant offset, all velocity profiles are referenced to a level of no motion at approximately 300–500 m depth which corresponds to the interface between North Atlantic central water and the Mediterranean water, which flow in opposite directions.

The velocities are shown contoured on a plot of depth versus distance across the outflow. We compared contour plots of direct and calculated velocities for sections D, E, and F (see Figure 1.1) and lines 4, 8, and 17 (see Figure 4.4.1). Qualitatively, the agreement between XCP- and CTD-derived velocities is good. In general, the patterns of distribution of inflow and outflow are similar, although in two sections (section D and line 8) the agreement was not as good. In section D (Figure 4.4.2), the curvature of the Mediterranean outflow may introduce some deviation from a geostrophic balance; in line 8 (Figure 4.4.3), the presence of a Meddy at the southern end of the section (left on the plot) is observed in the XCP data but not in the geostrophic section, since the flow is in cyclo-geostrophic balance.

Section 4.4 was contributed by Jane A. Verrall, Applied Physics Laboratory,
University of Washington, and Isabel Ambar, University of Lisbon.
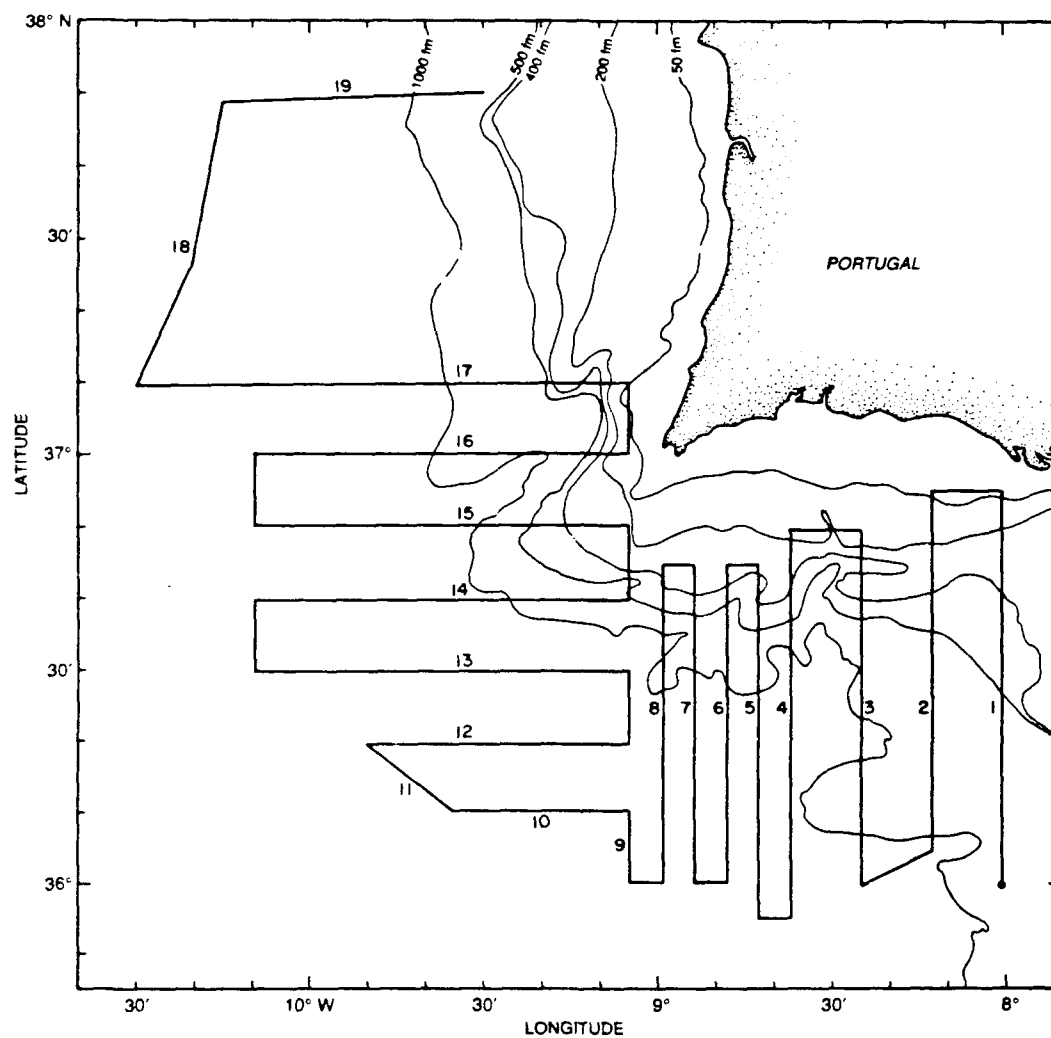
**Figure 4.4.1** Survey pattern for Meddy component.

XCP Velocities (cm/s) Normal to Section D

2565 2564 2563 2552 2551 2550 2549

Geostrophic Velocities (cm/s) Section D

87/88 88/87 85/86 84/85 83/84 82/83 81/82

Figure 4.4.2. EM velocities from XCPs (top) and geostrophic velocities from CTDs (bottom) for Section D. Positive velocities indicate westward outflow of Mediterranean water. The right side of the plot is closest to shore.

XCP Velocities (cm/s) Normal to Line 8

Geostrophic Velocities (cm/s) Line 8
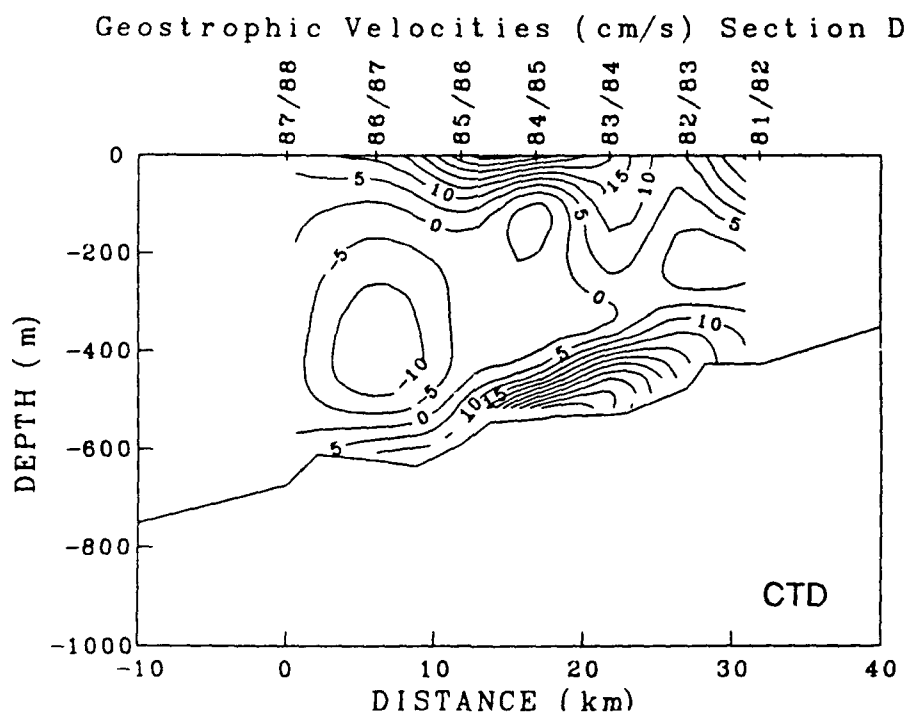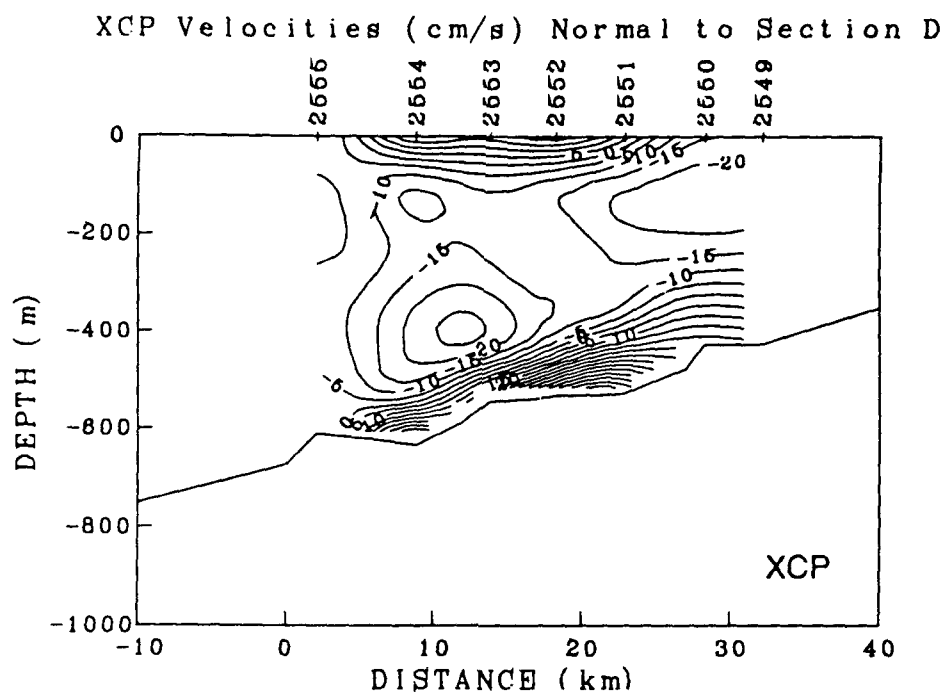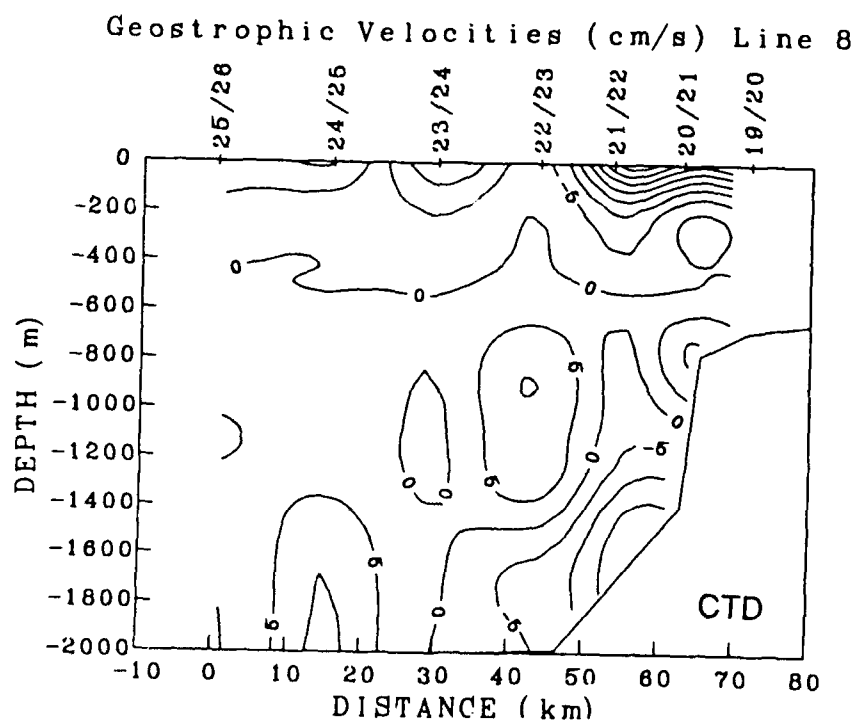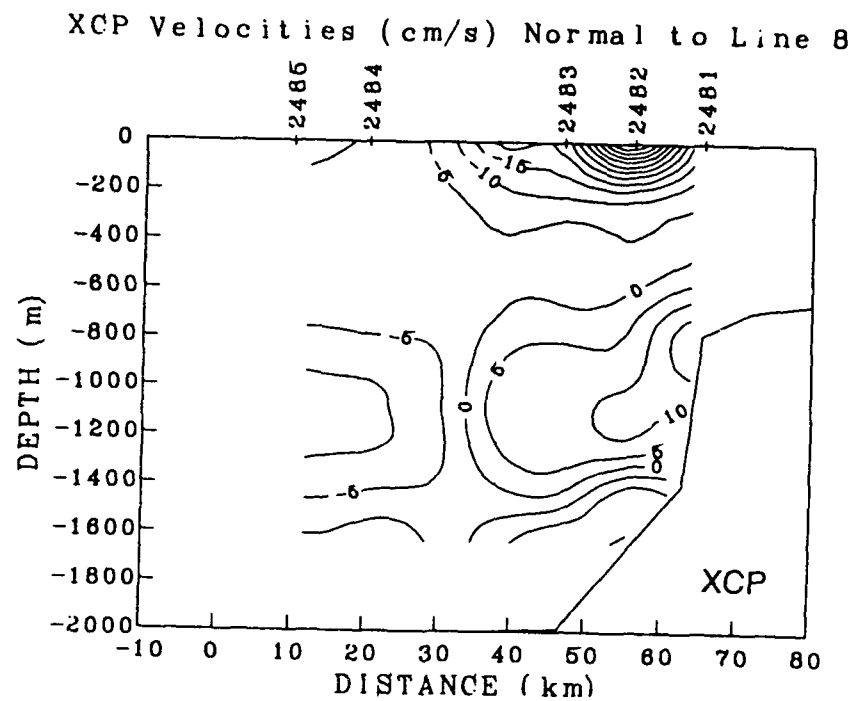

Figure 4.4.3. EM velocities from XCPs (top) and geostrophic velocities from CTDs (bottom) for line 8. Positive velocities indicate westward outflow of Mediterranean water. The right side of the plot is closest to shore.

5. RELATED WORK

5.1 Secondary Circulation in the Faeroe Bank Channel Outflow

Data from three expendable current profilers (XCPs) dropped at the center of the sill of the Faeroe Bank Channel and a CTD station occupied there (Figure 5.1.1) are used to examine the structure of the northwestward outflow of cold, fresh, dense water from the Norwegian Sea through the channel into the Atlantic Ocean. The velocity profiles are made barotropic and decomposed into downstream (311°T) and cross-stream (41°T) components. Downstream is defined as the direction of the difference between the mean velocity from 100–200 m (in the upper water) and that from 650–750 m (at the nose of the outflow). The resulting, very similar, profiles are averaged as a function of height above the bottom to obtain a mean profile (Figure 5.1.2).

A mixed Ekman and logarithmic bottom boundary layer is present in the bottom 120 m (Figure 5.1.2). A bottom stress of 3.4 ± 0.1 Pa is estimated using velocity observations from the individual unsmoothed profiles in the well-mixed log layer (30 m thick and directed $23 \pm 4°$ west of the downstream direction). This strong stress at the bottom boundary creates an Ekman layer in the bottom 120 m, and thus a secondary cross-stream flow to the southwest there. Spin-down times for the outflow estimated from the log and Ekman layer structures are 9 and 17 hours respectively. The outflow takes about 26 hours to flow through the channel, or 1.5–3 spin-down times. Thus the strong bottom friction must be important in the dynamics of flow through the channel.

The shear at the interface between the outflow water and the water above is sufficiently strong to overcome the stratification and generate Kelvin-Helmholtz billows at 500–600 m depth (where 75% of the values of the gradient Richardson number fall between 1/2 and 1/8). A cross-stream flow of similar magnitude to that in the bottom boundary layer but to the northeast is found in this high shear region at the interface. If persistent, this circulation may explain the pinching of the density field observed at the southwest channel wall in CTD sections across the channel. Cross-stream flow toward the southwestern wall of the channel in the bottom boundary layer would tend to pinch isopycnals there, while a cross-stream flow in the opposite direction at the interface combined with the possible mixing there would tend to spread the isopycnals to the northeast.

Section 5.1 was contributed by Gregory C. Johnson,
Applied Physics Laboratory, University of Washington.
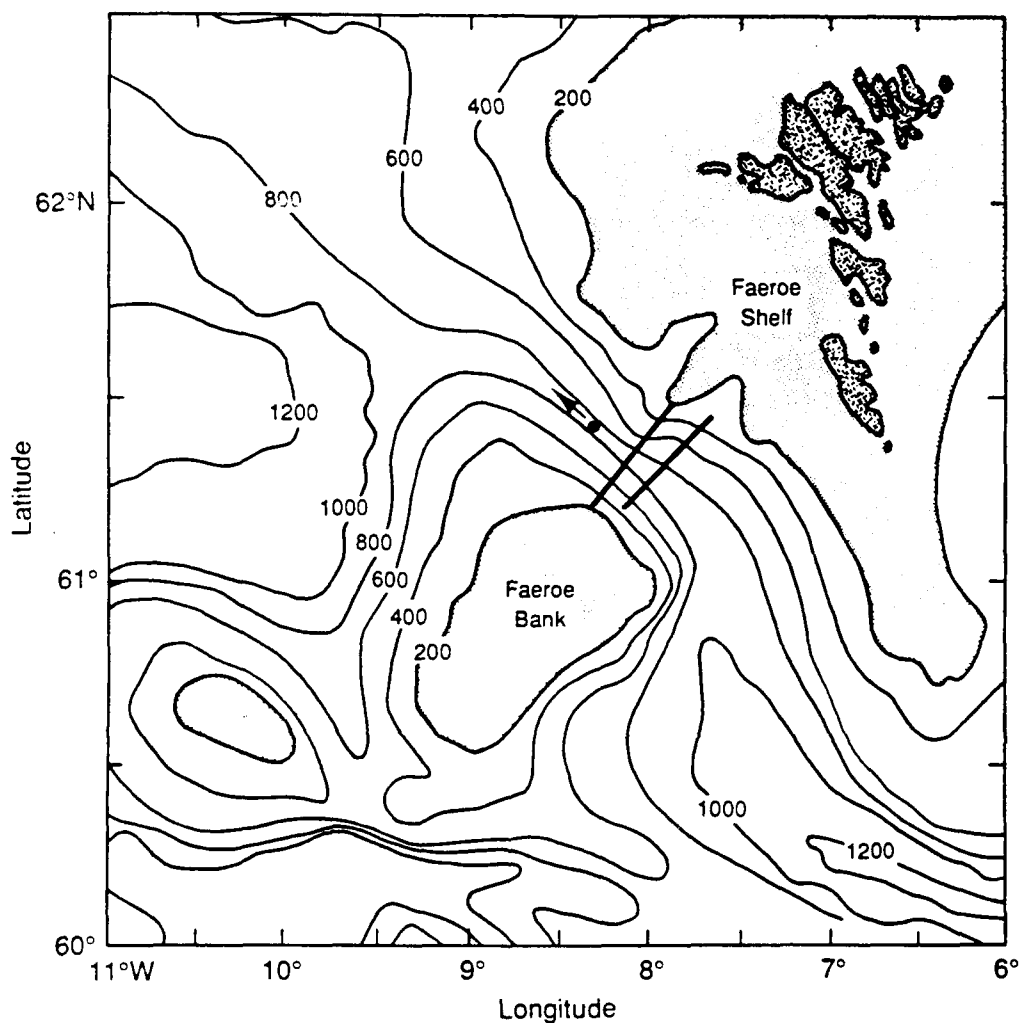
Figure 5.1.1. The bathymetry of the Faeroe Bank Channel (contours are in meters). The location of the CTD station and XCP drops at the center of the channel sill (61.43°N, 8.34°W) is indicated by large dot. The arrow indicates the downstream coordinate axis 311°T, which is aligned approximately with the isobaths. Dark lines represent locations of CTD sections across the channel.
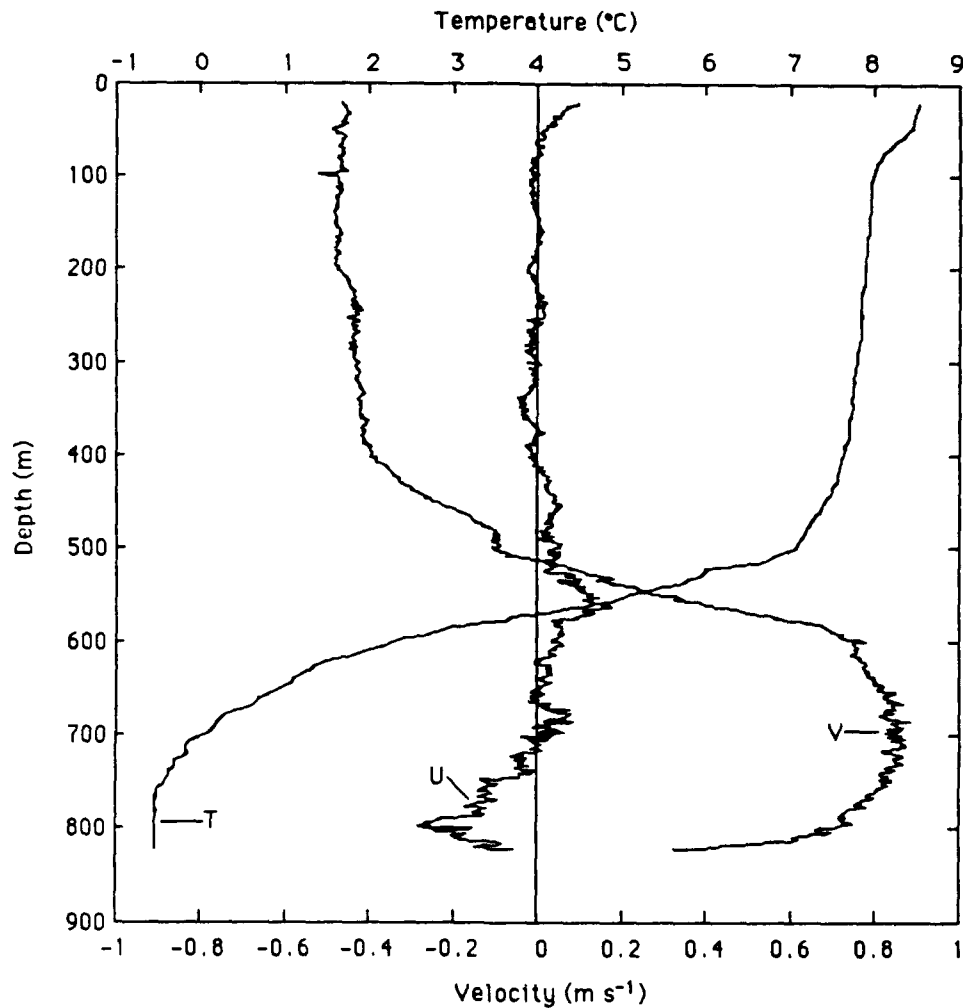
Figure 5.1.2. The mean 2-m smoothed temperature (T), downstream velocity (V, 311°T), and cross-stream velocity (U, 41°T) profiles plotted against depth. The stratification of the interface between the warm upper layer and the colder outflow water is strongest between 500 and 600 m. Below about 750 m in the bottom boundary layer (BBL), the temperature is homogeneous. The outflow water moves downstream and the water above upstream with a strong vertical shear between them. Downstream velocity decreases below about 700 m, in the BBL. Significant cross-stream velocities are observed at the depths of strong downstream shear, the interface, and the BBL.

5 2 Turbulence and Mixing in the Strait of Gibraltar

Two cruises in the strait were undertaken as part of the Gibraltar Experiment, to study the influence of turbulence and mixing on the two-layer exchange flow in the strait and to examine the characteristics of turbulence in the energetic strait regime. The surveys in the strait (with over 1100 microstructure profiles) were carried out October 12–20, 1985, and May 4–16, 1986. Results from the cruises (sampling of temperature, conductivity, and small-scale velocity, as well as ship-mounted velocity measurements and echosounder profiling in the upper 275 m) were analyzed.

Mixing accounts for the changes in the inflowing layer along the strait. In the west end, the inflow layer is virtually pure Atlantic water. In the total inflow of 1.2 Sv observed at the east end, 0.4 Sv is unchanged Atlantic water, and 0.8 Sv is half Atlantic and half entrained Mediterranean water. The CTD and velocity data are used to predict turbulent and mean transport across isopycnals due to entrainment between the inflow and outflow layers. We use this estimate to predict buoyancy fluxes. We predict an average dissipation rate ε of 4×10^{-5} W kg^{-1} in the middle layer, which agrees fairly well with our observations but is higher than the average dissipation rate observed. The high dissipation and mixing at the Camarinal Sill are nearly enough to account for predicted buoyancy fluxes. The data set shows the importance of a thick interfacial layer (60–120 m) and the noncoincidence of the velocity and density interfaces. Because of tidal flows, velocity and density structure are highly variable, complicating analysis of water mass change within any short sequence of profiles.

The key high-dissipation region is the internal hydraulic jump at Camarinal Sill, which was sampled repeatedly. Peak dissipation rates observed at the jump were $>10^{-2}$ W kg^{-1} in a 10 m thick layer. (See Figure 5.2.1 for an example of a transit through an internal jump.) Overturns downstream of the jump were often greater than 50 m thick. A second important source of mixing is internal bores propagating eastward, which were also sampled repeatedly. (Figure 5.2.2 shows a burst which sampled an internal bore. Figure 5.2.3 shows the contrast in profiles taken just before and after the passage of the bore.) The dissipation signal in the bores decays fairly rapidly; samples 15 km and 25 km east of the sill are markedly different.

Turbulence in the strait was extremely high, typically 2 to 4 orders of magnitude higher than in open-ocean thermocline samples. Dissipation rates were highly variable and could not be parameterized in terms of the shear observed in ADCP profiles. Thorpe and Ozmidov scales are nearly equal.

Velocity and density data from the east end of the strait show that the exchange was different in October than in May—it was submaximal in October and maximal in May.

Section 5.2 was contributed by Joel C. Wesson,
Applied Physics Laboratory, University of Washington.
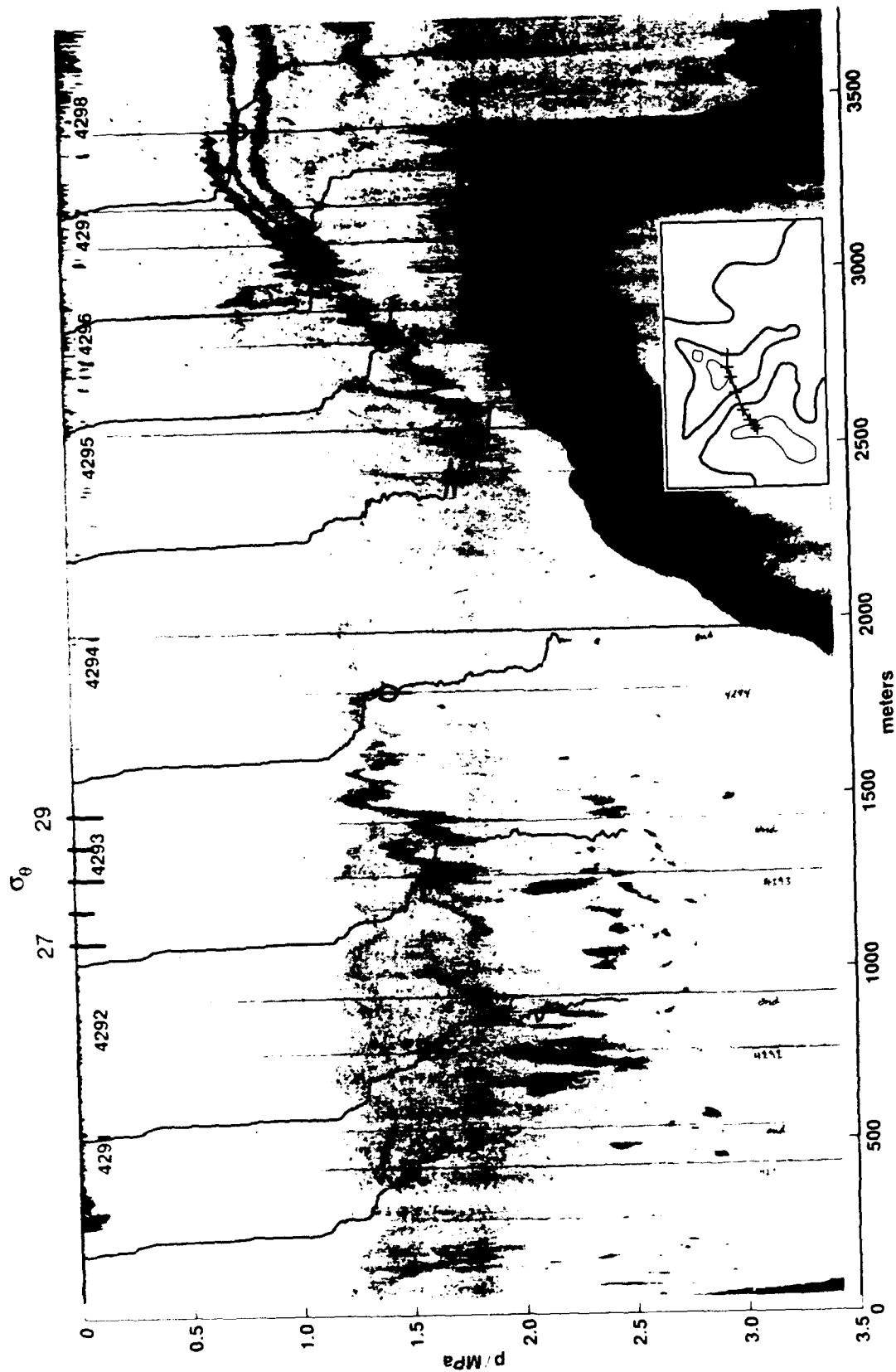
Figure 5.2.1. Echosounder image and overlaid density profiles for burst 84, taken May 14, 1986, over Camarinal Sill between 4 and 3 hours before high water. The interface is extremely thin east of the sill (right), breaks up in instabilities over the sill, and is quite broad west of the sill. Peak dissipation rates are always in the middle and lower layers and just west of the sill.
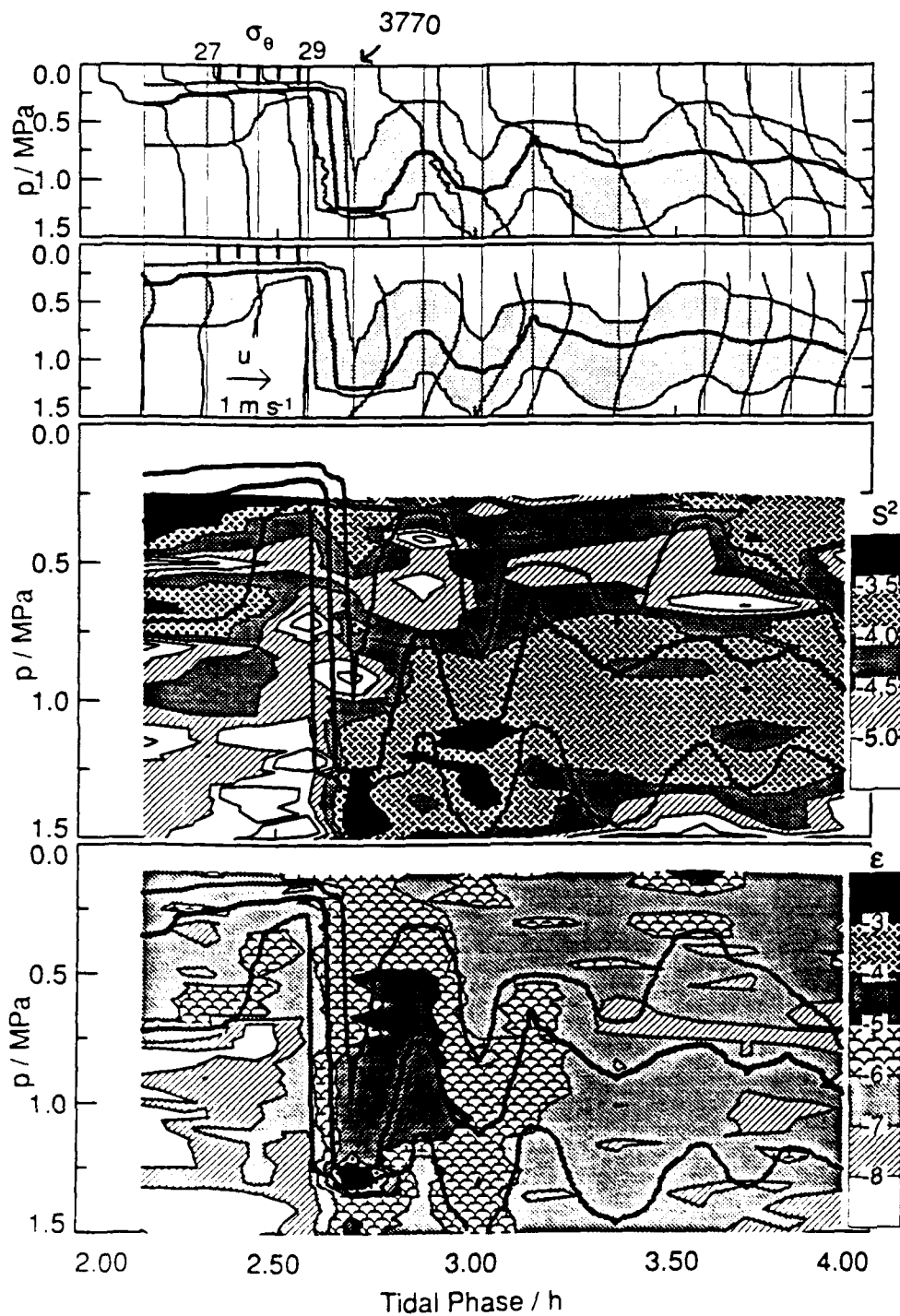
Figure 5.2.2. Burst summary during the passage of an internal bore (burst 42). This burst was taken in Tarifa Narrows, about 12 km east of Camarinal Sill, on May 9, 1986. In the upper two panels the density and velocity change dramatically when the bore arrives. In the lower two panels S^2 and ϵ also change substantially.
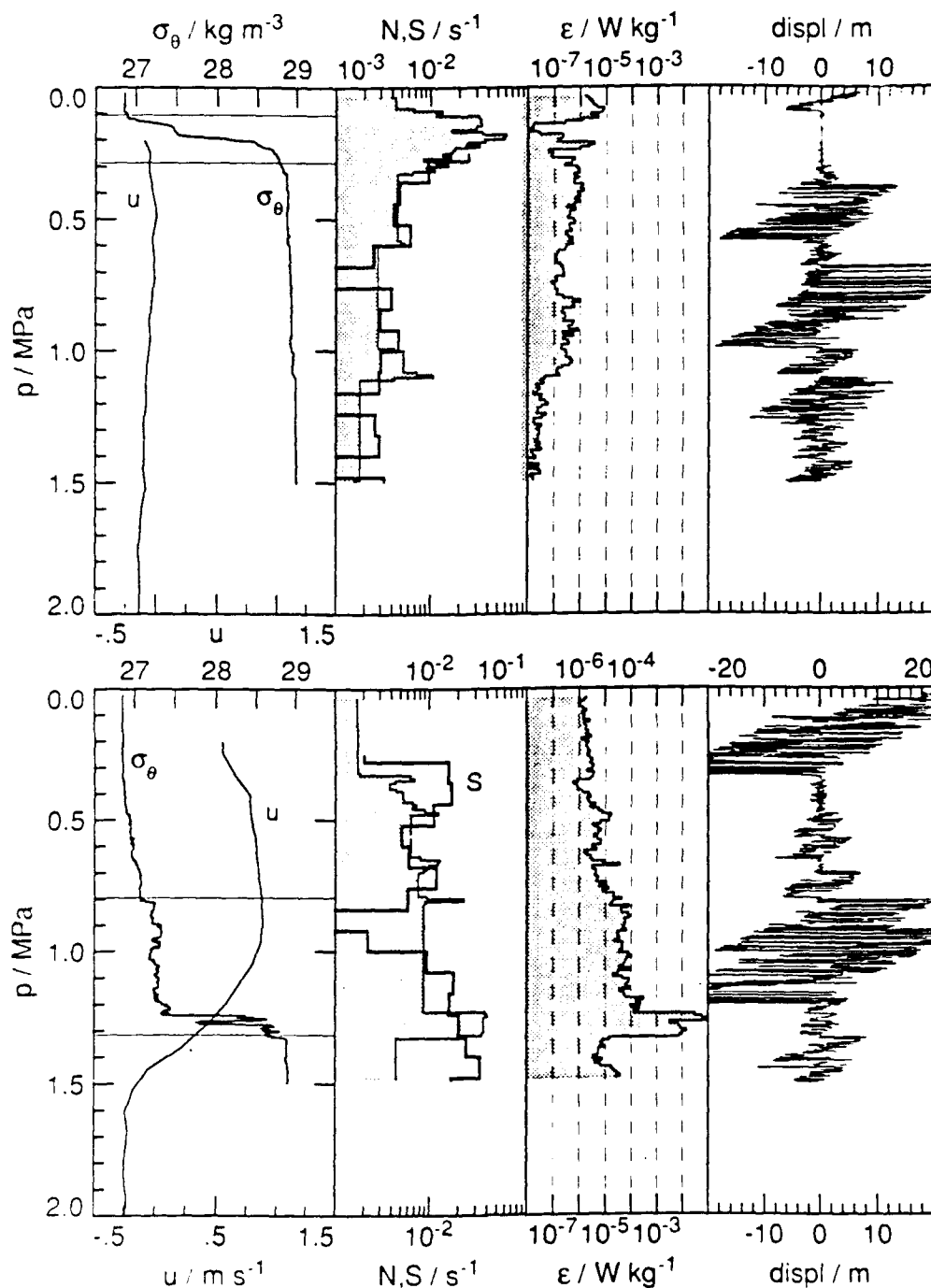
Figure 5.2.3. Profile summaries before and after the bore's arrival, drops 3769 and 3770 in burst 42. The key changes between the two profiles are the interface depth and the dissipation rates. In the last panel, large Thorpe displacements are in the upper layer and the interface layer after the bore arrives but only in the nearly unstratified lower layer before the bore.

5.3 Kiel Plans—Lagrangian Observations in the Mediterranean Outflow in the Iberian Basin

The tongue of Mediterranean water in the northeastern Atlantic has been a research topic at the Institut für Meereskunde (IfM) for two decades. In 1988, we proposed to one of our funding agencies, the Deutsche Forschungsgemeinschaft, to introduce a Lagrangian method to study advection of, and mixing within, the plume of Mediterranean water. By courtesy of Tom Rossby and his team at the University of Rhode Island, we had the opportunity to transfer the RAFOS technology to the IfM in Kiel. This Lagrangian method uses neutrally buoyant glass floats (1.6 m long, 11 liter displacement) to trace the Mediterranean water *in situ*. Acoustic underwater communication enables RAFOS floats to collect travel-time data of coded signals from at least two fixed sound sources. This information, together with pressure and temperature data, provides the initial input for the calculation of three-dimensional trajectories of Mediterranean water parcels (Figure 5.3.1).

During the past two years, we have built up a float group in Kiel. We have learned to build RAFOS floats (Figure 5.3.2), calibrate, and ballast them, and we have successfully tested our instruments. Presently we are preparing for an experiment to be carried out from aboard our research vessel, *Poseidon*, in the Iberian Basin in late May 1991. We plan to launch floats in the undercurrent off the continental rise and in potential salt lenses to be identified by Rolf Käse and his modeling group. They left Kiel for their studies in the Iberian Basin in late March 1991.

As already suggested in the original proposal from 1988, we plan to continue our work with repeated float deployments. We have asked the Deutsche Forschungsgemeinschaft to extend our funding through next year. We plan repeated float seedings from a location south of the Portuguese Algarve Coast at intervals of about 10 days. We would like to track the upper and the lower cores of Mediterranean water from their virtual source in the outer Gulf of Cadiz, where the tongue loses its contact with the sea floor. This project will be open to constructive cooperation if we get the necessary funding. The offer is especially attractive because the ensonification of the area in the Iberian Basin could be utilized by an unlimited number of floats. According to our present plans, the sound array may consist of up to four moored sound sources, jointly supplied by IfM Kiel and Ifremer Brest.
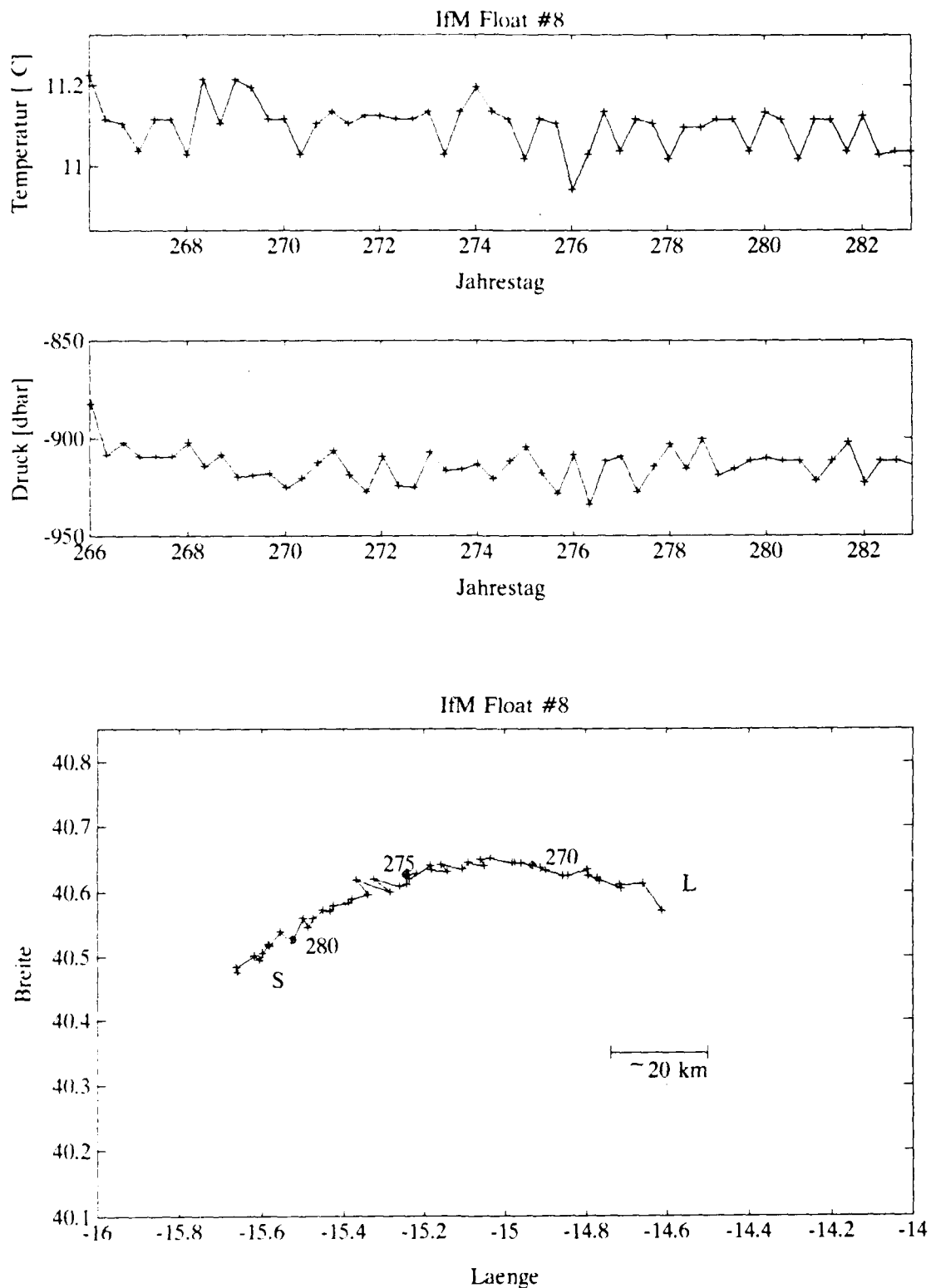
Figure 5.3.1. Example of a RAFOS float record from the Iberian Basin. On top and in the middle, we show time series of temperature and pressure records during a 17-day test occurring in fall 1990. The trajectory on the bottom has been calculated from only two functioning sound sources. L and S denote the launch site and the spot where the recovered float was first seen by the ARGOS satellite system. A vector-averaged speed on the order of $5\,cm\,s^{-1}$ was determined for the background field of the Mediterranean water tongue.

Figure 5.3.2. RAFOS float production in Kiel. The glass floats were assembled, tested, calibrated, and ballasted before shipment to Lisbon. We plan to launch them in the Iberian Basin in May 1991.

REFERENCES

Ambar, I., A. Bower, A. Cantos-Figuerola, M. A. Kennelly, E. L. Kunze, R. Lueck, M. T. O'Neil Baringer, G. Parrilla, M. D. Prater, J. F. Price, P. L. Richardson, T. B. Sanford, and K. S. Tokos, 1990: Report on the Gulf of Cadiz Expedition Workshop, October 1 & 2, 1989. APL-UW TM 9-90, Applied Physics Laboratory, University of Washington, Seattle, WA, 58 pp.

Armi, L., D. Hebert, N. Oakey, J. F. Price, P. L. Richardson, H. T. Rossby, and B. Ruddick, 1989: Two years in the life of a Mediterranean salt lens, *J. Phys. Oceanogr.*, **19**, 354–370.

Chriss, T. M., and D. R. Caldwell, 1982: Evidence for the influence of form drag on bottom boundary layer flow, *J. Geophys. Res.*, **87**, 4148–4154.

D'Asaro, E. 1988: Generation of submesoscale vortices: A new mechanism, *J. Geophys. Res.*, **93**, 6685–6693.

Dewey, R. K., and W. R. Crawford, 1988: Bottom stress estimates from vertical dissipation rate profiles on the continental shelf, *J. Phys. Oceanogr.*, **18**, 1167–1177.

Griffiths, R. W., and P. F. Linden, 1981: The stability of buoyancy-driven coastal currents, *Dynamics of Atmospheres and Oceans*, **5**, 281–306.

Gust, G., and G. L. Weatherly, 1985: Velocities, turbulence and skin friction in a deep-sea logarithmic layer, *J. Geophys. Res.*, **90**, 4779–4792.

Hebert, D., N. Oakey, and B. Ruddick, 1990: Evolution of a Mediterranean salt lens: Scalar properties, *J. Phys. Oceanogr.*, **20**, 1468–1483.

Heezen, B. C., and G. L. Johnson, 1969: Mediterranean undercurrent and microphysiography west of Gibraltar, *Bull. Inst. Oceanogr. (Monaco)*, **67**(1382), 1–97.

Madelain, F., 1970: Influence de la topographie du fond sur l'écoulement Méditerranéen entre le Détroit de Gibraltar et le Cap Saint-Vincent, *Cah. Oc.*, **22**, 43–61.

McWilliams, J. C., 1988: Vortex generation through balanced adjustment, *J. Phys. Oceanogr.*, **18**, 1178–1192.

Nof, D., 1991: Lens generated by intermittent currents, *Deep-Sea Res.*, **38**, 325–345.

Zenk, W., 1975: On the Mediterranean outflow west of Gibraltar, *"Meteor" Forsch.-Ergebn.*, ser. A, **16**, 23–24.

APPENDIX A

Agenda

Gulf of Cadiz Workshop II
April 9–11, 1991
Applied Physics Laboratory
University of Washington

Gulf of Cadiz Workshop II
April 9-11, 1991
Applied Physics Laboratory
University of Washington

Day 1: Tuesday, April 9

Registration (coffee and pastry)	0830-0845
Introduction	0845-0900

    - Administrative Matters (Sanford)
    - Workshop Goals (Sanford)

Principal Investigator/(Cruise Participant) Talks

- Data Overview (Kennelly)	0900-0930
- Ertel Vorticity Finestructure near Ampere Seamount (Kunze)	0930-1030
Break	1030-1045
- Dynamical Aspects of the Cadiz Meddy and Hypotheses of Generation (Prater)	1045-1145
Lunch	1145-1300
- Bottom Stress in the Mediterranean Plume (Sanford)	1300-1400
- Viscous Bottom and Total Stress in the Mediterranean Plume (Lueck)	1400-1500
Break	1500-1515
- Modeling the Mediterranean Outflow (Price)	1515-1545
- The Mediterranean Overflow: an Overview (Baringer)	1545-1615
Group Dinner	1900-

Day 2: Wednesday, April 10

Coffee and Pastry	0830-0845

Other Talks

- Secondary Circulation in the Faeroe Bank Channel Outflow (Johnson)	0845-0915
- Mixing in the Strait of Gibraltar: Overview and Phenomena (Wesson)	0915-0945

Break	0945-1000
Plans for the Lisbon Meeting (Sanford)	1000-1045
Workshop Report Discussion (Kennelly) - Outline	1045-1130
Lunch	1130-1230
Large Scale Structure of the Mediterranean Overflow (Baringer) Wednesday Physical Oceanography Lunch Seminar Marine Sciences Building (MSB) Room 123	1230-1330
Reception: South Campus Center Crow's Nest Room 354	1330-1530
Oceanic Overflows (Price) Wednesday Oceanography Seminar Oceanography Teaching Building (OTB) Room 14	1530-1630
Dinner	1900-

Day 3: Thursday, April 11

Comparison of Velocities from CTD Sections   0900-0930
with XCP Sections (Verrall)

The Future (Group)   0930-
    - Expected Papers
    - Other Meetings
    - FY92-93 Funding Considerations
    - Experiments

Group Discussion

Close of Meeting   1200

APPENDIX B

List of Contributions
Resulting from the Gulf of Cadiz Expedition

1. Kennelly, M. A., J. H. Dunlap, T. B. Sanford, E. L. Kunze, M. D. Prater, and R. G. Drever, 1989: The Gulf of Cadiz Expedition: R/V *Oceanus* Cruise 202. APL-UW TR 8914, Applied Physics Laboratory, University of Washington, Seattle, WA, 115 pp.

2. Kennelly, M. A., T. B. Sanford, and T. W. Lehman, 1989: CTD Data from the Gulf of Cadiz Expedition: R/V *Oceanus* Cruise 202. APL-UW TR 8917, Applied Physics Laboratory, University of Washington, Seattle, WA, 129 pp.

3. Kennelly, M. A., M. D. Prater, and T. B. Sanford, 1989: XBT and XSV Data from the Gulf of Cadiz Expedition: R/V *Oceanus* Cruise 202. APL-UW TR 8920, Applied Physics Laboratory, University of Washington, Seattle, WA, 209 pp.

4. Kennelly, M. A., M. D. Prater, J. H. Dunlap, E. L. Kunze, and T. B. Sanford, 1989: XCP Data from the Gulf of Cadiz Expedition: R/V *Oceanus* Cruise 202. APL-UW TR 8925, Applied Physics Laboratory, University of Washington, Seattle, WA, 206 pp.

5. Lynch, J., and R. Lueck, 1989: Expendable Dissipation Profiler (XDP) Data from the Mediterranean Out-Flow Experiment: R/V *Oceanus* Cruise 202 Leg V. JHU-CBI TR 89-01, Johns Hopkins University, Chesapeake Bay Institute, Baltimore, MD, 284 pp.

6. Price, J. F., and M. T. O'Neil [Baringer], 1988: The descending Mediterranean plume (abstract). *Eos Trans. AGU,* 69(44), 1265.

7. Prater, M. D., and T. B. Sanford, 1989: Observations of an intense, young Meddy (abstract). *Eos Trans. AGU,* 70(43), 1159.

8. Ambar, I., A. Bower, A. Cantos-Figuerola, M. A. Kennelly, E. L. Kunze, R. Lueck, M. T. O'Neil Baringer, G. Parrilla, M. D. Prater, J. F. Price, P. L. Richardson, T. B. Sanford, and K. S. Tokos, 1990: Report on the Gulf of Cadiz Expedition Workshop, October 1 & 2, 1989. APL-UW TM 9-90, Applied Physics Laboratory, University of Washington, Seattle, WA, 58 pp.

9. Prater, M. D., and T. B. Sanford, 1990: Generation of Meddies off Cape St. Vincent, Portugal (abstract). *Eos Trans. AGU,* 71, 1416.

10. Prater, M. D., 1991: A method for depth and temperature correction of expendable probes. *J. Atmos. Ocean. Tech.* (in press).

11. Ambar, I., and J. Verrall, 1990: Dynamics of the Mediterranean water plume between the Strait of Gibraltar and Cape St. Vincent, *Proceedings of the 7th National Conference on Physics* (Portugal), p. 457.

12. Kunze, E., and T. B. Sanford, 1990: Vorticity and horizontal divergence finestructure near a seamount (abstract). *Eos Trans. AGU*, 72(43), 1419.

13. Kunze, E., and T. B. Sanford, 1991: Measurements of ertel vorticity finestructure in the eastern North Atlantic. *Dynamics of Oceanic Internal Gravity Waves, Proceedings,* Peter Müller, Ed., Hawaii Institute of Geophysics (in press).

14. Baringer, M. O., and J. F. Price, 1990: A simple model of the descending Mediterranean outflow plume. *The Physical Oceanography of Sea Straits,* L. J. Pratt, Ed., Kluwer Academic Publishers, Netherlands, 537–544.

15. Price, J. F., and M. O. Baringer, 1990: A model of the Denmark Strait overflow (abstract). *Annales Geophysicae,* XV General Assembly, European Geophysical Society, Copenhagen, April 23–27, 1990, p. 224.

16. Baringer, M. O., J. F. Price, and T. B. Sanford, 1990: Mixing in the Mediterranean outflow plume during the Gulf of Cadiz Experiment (abstract). *Annales Geophysicae,* XV General Assembly, European Geophysical Society, Copenhagen, April 23–27, 1990, p. 224.

17. Parrilla, G., and A. Cantos-Figuerola, 1990: The Mediterranean outflow plume during the Gulf of Cadiz Experiment (Sept 1988) (abstract). *Annales Geophysicae,* XV General Assembly, European Geophysical Society, Copenhagen, April 23–27, 1990, p. 224.

18. M. D. Allison, I. Ambar, G. C. Johnson, M. A. Kennelly, H. König, E. L. Kunze, R. Lueck, M. O. Baringer, M. D. Prater, J. F. Price, T. B. Sanford, K. L. Schultz Tokos, J. Verrall, J. C. Wesson, and W. Zenk, 1991: Report on the Second Gulf of Cadiz Expedition Workshop, April 9–11, 1991. APL-UW TM 6-91, Applied Physics Laboratory, University of Washington, Seattle, WA.

19. Kunze, E., M. A. Kennelly, and T. B. Sanford, 1991: The depth dependence of shear finestructure off Point Arena and over Pioneer Seamount, *J. Phys. Oceanogr.,* 21 (in press).

APPENDIX C

List of Participants
Gulf of Cadiz Workshop
April 9–11, 1991

Gulf of Cadiz Workshop II Participants

Dicky Allison
Applied Physics Laboratory
University of Washington
1013 NE 40th Street
Seattle, WA 98105
206-543-9829
email: allison@apl.washington.edu
telemail: d.allison

Molly O'Neil Baringer
Clark 2
Woods Hole Oceanographic Institution
Woods Hole, MA 02543
508-548-1400 X2683
email: oneil@rascals.whoi.edu

Eric D'Asaro
Applied Physics Laboratory
University of Washington
1013 NE 40th Street
Seattle, WA 98105
206-685-2982
email: dasaro@apl.washington.edu
telemail: e.dasaro

John Dunlap
Applied Physics Laboratory
University of Washington
1013 NE 40th Street
Seattle, WA 98105
206-543-7207
email: dunlap@apl.washington.edu

Greg Holloway
Institute of Ocean Science
P.O. Box 6000
Sidney, B.C., V8L4B2
Canada
604-363-6564
email: greg@ocean.washington.edu
telemail: ios.bc

Mike Gregg
Applied Physics Laboratory
University of Washington
1013 NE 40th Street
Seattle, WA 98105
206-543-1353
email: gregg@apl.washington.edu
telemail: m.gregg

Gregory C. Johnson
Applied Physics Laboratory
University of Washington
1013 NE 40th Street
Seattle, WA 98105
206-685-3994
email: johnson@apl.washington.edu

Maureen Kennelly
Planning Systems, Inc.
7925 Westpark Drive
McLean, Virginia 22102
703-734-3437
email: kennelly@apl.washington.edu
telemail: m.kennelly
FAX: 703-734-3456

Eric Kunze
Oceanography, WB-10
University of Washington
Seattle, WA 98195
206-543-8467
email: kunze@narwhal.ocean.washington.edu
telemail: e.kunze

Tom Lehman
Applied Physics Laboratory
University of Washington
1013 NE 40th Street
Seattle, WA 98105
206-543-0215
email: lehman@apl.washington.edu

Rolf Lueck
Centre for Earth & Ocean Research
University of Victoria
P.O. Box 3055
Victoria, B.C., V8W 3P6
Canada
604-721-8918
email: rolf@george.uvic.ca
telemail: r.lueck
FAX: 604-721-7715

Mark Prater
Applied Physics Laboratory
University of Washington
1013 NE 40th Street
Seattle, WA 98105
206-543-7886
email: prater@apl.washington.edu

Jim Price
Woods Hole Oceanographic Institution
Woods Hole, MA 02543
508-548-1400 X2526
email: jim@buckwheat.whoi.edu
telemail: j.price.whoi

Tom Sanford
Applied Physics Laboratory
University of Washington
1013 NE 40th Street
Seattle, WA 98105
206-543-1365
telemail: t.sanford
email: sanford@apl.washington.edu
FAX: 206-543-6785

Jane Verrall
Applied Physics Laboratory
University of Washington
1013 NE 40th Street
Seattle, WA 98105
206-543-7886
email: verrall@apl.washington.edu

Joel Wesson
Applied Physics Laboratory
University of Washington
1013 NE 40th Street
Seattle, WA 98105
206-543-1256
email: wesson@apl.washington.edu

APPENDIX D

Planned Presentations of Gulf of Cadiz Expedition Data

APPENDIX D

Planned Presentations of Gulf of Cadiz Expedition Data

1 & 2 October 1989   Gulf of Cadiz Expedition Workshop,
                      Woods Hole, Massachusetts, USA

9–11 April 1991   Second Gulf of Cadiz Expedition Workshop,
                      Seattle, Washington, USA

1–4 October 1991   International Workshop on Outflows and Overflows
                      in the Atlantic and Their Role
                      in the Eastern Boundary Current System,
                      Lisbon, Portugal

27–31 January 1992   AGU Ocean Sciences Meeting, Special Session:
                      Overflows and Outflows,
                      New Orleans, Louisiana, USA